2023 Data Collection with the NSSL Advanced Technology Demonstrator

Lead Author: Addison Alford[1]

Contributors: Charles Kuster[1], Terry Schuur[2,1], Anthony Reinhart[1], Jami Boettcher[2,1], Jacob Carlin[2,1], Arthur Witt[1], Chris Curtis[2,1], Robbie Estes[2,1], Eddie Forren[2,1], Stephen Gregg[2,1], Larry Hopper[1], Igor Ivić[2,1], Feng Nai[2,1], Patrick Servello[2,1], Chad Smith[1], Sebastián Torres[2,1], David Warde[2,1], Danny Wasielewski[1], Felicia Woolard[1], Allen Zahrai[2,1], and Noah Zemlin[2,1]

[1]NOAA/OAR/National Severe Storms Laboratory; Norman, OK; [2]Cooperative Institute for Severe and High-Impact Weather Research and Operations, University of Oklahoma; Norman, OK

U.S. Department of Commerce
National Oceanic and Atmospheric Administration
Office of Atmospheric Research
National Severe Storms Laboratory

Contents

List of Figures

List of Tables

1. Executive Summary

The Advanced Technology Demonstrator (ATD) is a dual-polarization phased array radar (PAR) that is operated by the National Oceanic and Atmospheric Administration (NOAA) National Severe Storms Laboratory (NSSL). The ATD is the first full-scale, S-band polarimetric PAR designed for weather observations to test the feasibility of PAR as a potential next generation radar system in the United States. Polarimetric PAR has been met with challenges related to the cross-polarization isolation, which can bias radar measurements when the beam is steered off center. However, polarimetric PAR has rapidly matured in the past decade, in part due to engineering advancements made aboard the ATD.

Weather radar is positioned to benefit from polarimetric PAR through, for example, rapid updates of quickly evolving severe weather, greater spatial coverage (particularly through the use of dense elevation angles), and tremendous flexibility through operating modes that can capture observations very quickly and/or in a very focused manner. The ATD has been operational since 2020, collecting 37 use cases between 2020 and 2022. In 2023, the ATD's case portfolio was more than doubled with a total of 57 use cases collected. Data collection by the ATD was driven by 1) demonstrating the quality of dual-polarization measurements of a well-calibrated PAR for use in research and operational settings, 2) demonstrating the utility of vertically dense observations, and 3) acquiring use cases for evaluation by operational meteorologists in the NOAA Hazardous Weather Testbed (HWT). Ultimately, each of the former objectives was satisfied through observing a variety of cases spanning severe and non-severe weather targets that include supercells, mesoscale convective systems, multicell convection, downbursts, winter weather, and clear-air events. Tornadoes, severe hail, severe winds, and flash flooding were observed across a span of convective modes. Thirteen of the 57 cases were identified as being suitable for potential future use in the HWT.

The cases collected in 2023 are actively being used for both research and operational evaluation. A particularly active area of investigation is the use of mid- and upper-level dual-polarization signatures that are precursors to severe hazards at the surface. Preliminary results have shown that the rapid and vertically dense observations from the ATD much better capture mid- and upper-level dual-polarization data while maintaining rapid low-level updates. Additionally, the ATD's dual-polarization measurements appear to contain significantly less noise (e.g., spatial variance of dual-polarization data) than other radar systems (e.g., the WSR-88Ds) that lead to improvements in radar data quality. Investigations are ongoing to evaluate how the combined dual-polarization data quality and dense spatiotemporal observations of ATD affect quantitative applications of radar measurements and warning and support decision making by operational meteorologists.

2. Background

2.1. The WSR-88D

Weather radar has long been used for monitoring, detecting, and evaluating severe weather hazards and convective and mesoscale processes (Doviak and Zrnić 2006). The National Weather Service (NWS) deployed the Weather Surveillance Radar - 1988 Doppler (WSR-88D) fleet in the early 1990s, which helped to revolutionize severe weather detection (Crum and Alberty 1993). In particular, the Doppler capabilities of the WSR-88D afforded forecasters the ability to detect wind shear associated with tornadic mesocyclones (e.g., Burgess et al. 1975), in addition to resolving atmospheric flow in severe and non-severe weather settings. An upgrade to WSR-88Ds to dual-polarization was begun in the early 2010s (Doviak et al. 2000) and completed in 2013, yielding improvements over single-polarization-based estimates of precipitation. Dual-polarization measurements procured the ability to differentiate hydrometeor types in thunderstorms, providing a more robust and comprehensive way to discriminate and quantify near-surface precipitation. Dual-polarization measurements also advanced the ability to detect tornadoes through the tornado debris signature (TDS; Ryzhkov et al. 2005).
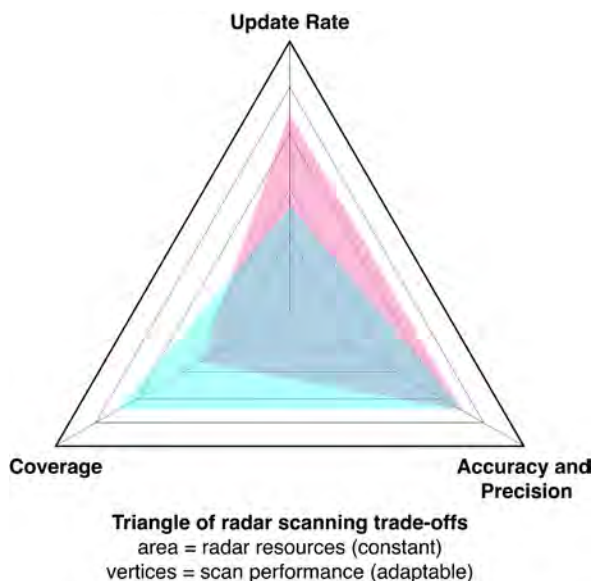
Figure 1. The radar triangle of scanning trade-offs. The figure illustrates that for a change in the vertex of the triangle, the other vertices must be changed such that the area of the triangle must be constant.

The WSR-88D, as with most weather radars, are mechanically steered systems. Depending on the observational objective, Fig. 1 displays the balance mechanically rotating radars must determine between collecting sufficient radar pulses or samples at a point in space to minimize measurement error (i.e., accuracy and precision), the

azimuth and elevation angles that will be sample (i.e., coverage), and the frequency of revisiting a point in space (i.e., the update rate). It is often desirable to increase the update rate to monitor rapidly evolving severe weather events such as supercells that may produce severe hail and tornadoes. It is also desirable to increase the vertical coverage of elevations sampled to detect the evolution of "precursor" signatures in the mid- and upper-levels of a storm that may later produce severe weather at the surface (e.g., Kuster et al. 2019).

2.2. Phased Array Radar

The NWS will complete an Analysis of Alternatives in 2027 to identify and analyze alternative solutions ahead of refining requirements and finalizing the next radar network design in 2032 that will replace the current national radar network using a phased approach by 2040. Although the operational requirements of the system are not yet fully known, the next radar system will likely maintain or improve the update rate, coverage, and accuracy and precision of radar measurements. To maximize the update rate without sacrificing data quality and/or coverage, rapidly rotating radars can leverage multiple transmit frequencies to maintain measurement accuracy (e.g., Pazmany et al. 2013). However, frequency allocation and required mechanical maintenance can be prohibitive to the broad adoption of such systems.
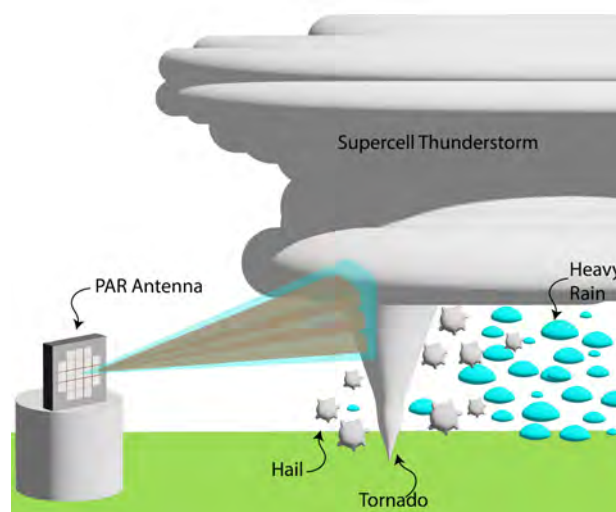
Fig. 2. A conceptual model of a PAR transmitting a spoiled beam (blue) and receiving three pencil beams (brown) to sample a supercell producing a tornado, hail, and heavy rain.

PAR is a candidate that offers tremendous flexibility to minimize (but not eliminate) the tradeoffs between the aforementioned limitations (Palmer et al. 2022). The update rate of a PAR is significantly increased due to electronic beam steering (versus mechanical). PAR can further increase the update rate through transmitting a wide beam and reconstructing individual beams upon receive (spoiled or imaging beam

operations; Fig. 2) or transmitting multiple beams simultaneously (beam multiplexing). Although the temporal update benefits of PAR are well known, the broad adoption of PAR in the atmospheric sciences has been slowed due to the difficulty of dual-polarization measurement calibration. Upon electronically steering the beam off broadside (i.e., the direction normal to the antenna face), cross-coupling between the horizontal and vertical polarized electromagnetic waves results in biases in dual-polarization measurements, most notably in differential reflectivity (Z_{DR}) and differential phase (ϕ_{DP}). Significant effort in recent years, however, has shown that robust calibration of off-broadside measurements is attainable (Ivić 2020, 2023). Therefore, PAR can maintain or improve dual-polarization measurement accuracy and precision relative to current operational radars. In addition, it can increase the spatial coverage of measurements by different means, such as the inclusion of additional azimuth and/or elevation angles, leveraging adaptive scanning techniques (e.g., focusing observations on a target of interest and reducing observations elsewhere), or a combination of the two.

Compared to mechanically-driven radars, there are relatively few PARs that are built for weather data collection and even fewer that leverage dual-polarization technology. However, NOAA NSSL built the ATD in the late 2010s to study polarimetric PAR. The ATD is a S-band, polarimetric PAR located in Norman, OK. It replaced the SPY-1A PAR, which was a single-polarization PAR leveraged by NSSL since the 2000s. With observations from the SPY-1A, the temporal updates of PAR were well documented through years of observations of severe convection, in addition to demonstrations of PAR-based capabilities such as adaptive scanning and advanced beamforming techniques (Zrnić et al. 2007; Heinselman et al. 2008, 2012, 2015; Newman and Heinselman 2012; Kuster et al. 2016; Stailey and Hondl 2016; Torres et al. 2016; Supinie et al. 2017; Stratman et al. 2020). Now, the ATD is in a similar position to illustrate the benefits of polarimetric PAR, including and beyond rapid-update benefits. Herein, the data collected by the ATD during calendar year (CY) 2023 are summarized with a particular focus on the spatial coverage and dual-polarization measurement accuracy.

3. The ATD in 2023

In 2023, the Phased Array Radar and Meteorological Analysis Studies Team (PAMST) was primarily responsible for weather data collection activities with the ATD. Leading up to the height of the 2023 severe weather season, three primary objectives were identified based on the then-current capabilities of the ATD:

(1) Observe severe storm hazards using novel, calibrated, dual-polarization, PAR observations that can both address research objectives and be used for operational evaluation.

(2) Evaluate the impacts of denser vertical sampling by adding additional elevation angles within typical operational scanning strategies in the context of rapid updates and in a dual-polarization framework.

(3) Build an archive of cases that can be used in future HWT experiments to examine the impacts of PAR data on operational meteorologist decision making and algorithm performance.

The ATD was operated in "pencil beam" mode (i.e., a single transmit and receive beam as a function of ATD's ~1.6° two-way beamwidth at broadside and 2.2° at ±45° azimuth relative to broadside) with a stationary antenna, which at most yielded a 90°-wide field of view in azimuth. Stationary, pencil beam operations mimic one side of a four-panel PAR concept, where a four-panel PAR would provide 360° azimuthal coverage. Forthcoming capabilities of the ATD are summarized later in section 5.4. A wide range of meteorological cases (severe and non-severe) were sought to achieve the above objectives. The 2023 data-collection season more than doubled the ATD case portfolio with more than 50 individual data-collection periods that focused on observing a wide range of meteorological phenomena including:

1) Tornadic supercells, with a focus on low-level rapid updates and rapid, high-vertical resolution volume coverage patterns (VCPs),

2) Severe and non-severe hail with VCPs that allow for a detailed examination of the mid- and upper-levels of severe convection in the hail growth zone,

3) A severe quasi-linear convective system (QLCS) that produced multiple tornadoes with VCPs that included rapid revisits in the low levels and dense low- and mid-level elevation cuts,

4) Winter weather events with dense low-level vertical sampling and rapid volumetric updates in convective sleet,

5) Downbursts with VCPs tailored to include additional elevation cuts in the mid and upper-levels to focus on precursor signatures such as specific differential phase (K_{DP}) cores and descending reflectivity cores,

6) Convective and stratiform rain for examining the dual-polarization data quality in quantitative precipitation estimation,

7) Stratiform rain for self-consistency testing of the ATD dual-polarization calibration, and

8) Severe and non-severe mesoscale convective systems.

Table 1 summarizes the number of cases sampled by the ATD delineated by each case's predominant target of interest.

Tornadic Supercells	Severe and Non-severe MCS	Severe Multicell Convection	Nonsevere Multicell Convection	Downburst	Winter Weather	Clear Air and Engineering Tests
3*	9*	10	19	4	2	11

Table 1. Storm-type event counts collected by the ATD in 2023. The asterisks under the supercell and MCS categories signifies that one particular case was counted both under the supercell and MCS category. Therefore, the total use cases collected is actually 57 with one case being split between the supercell and MCS categories.
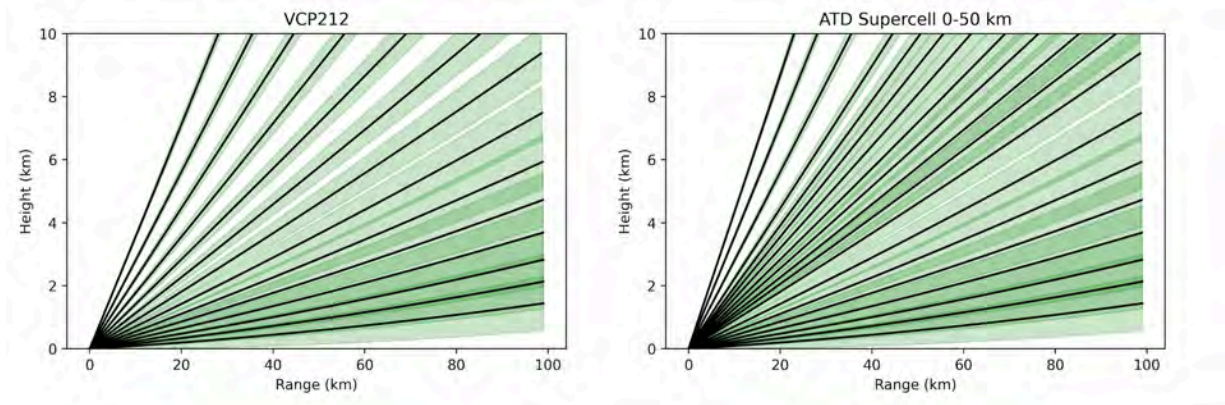
Figure 3. A comparison of (a) VCP 212 elevation angles and (b) ATD's Supercell VCP for storms between 0–50-km range. VCP 212 updates every 4.5 to 6-minutes whereas the ATD Supercell VCP takes ~1.5-minutes. The beamwidth is assumed to be 1.0°. ATD operates at a lowest elevation angle of 0.5° and can scan higher in elevation than the WSR-88Ds if desired as in the ATD Supercell VCP.

The VCPs with which the aforementioned cases were sampled were constructed with baseline the elevation angles used by VCP 212, which is often leveraged by the WSR-88Ds to monitor precipitation and severe hazards. With the ATD, vertical sampling was increased while exceeding the VCP update times afforded by the WSR-88Ds. For example, Fig. 3 shows the differences between VCP 212 (Fig. 3a) and the ATD Supercell VCP (Fig. 3b) for a tornadic supercell that is ideally placed at 0–50-km range from the ATD. The WSR-88Ds can eliminate upper elevation angles sampled to increase speed, but do not adjust directly the elevation angles sampled depending on the range of the target. The 2023 ATD Supercell VCPs (and similar VCPs for MCSs, severe hail storms, etc.) did account for the range of a target in order to optimize mid- and upper-level sampling. The ATD Supercell 0-50-km range VCP afforded a 90-s volume update time with denser vertical resolution (relative to VCP 212) and a 45-s update at 0.5° elevation. In contrast, VCP 212 takes approximately 5–6 minutes to complete and has a 90- to 150-s revisit time at the 0.5° elevation when leveraging SAILS cuts. Theoretically, the enhancement of vertical sampling with ≤90-s updates affords 1) better detection of hail growth aloft and its subsequent descent, 2) better detection of rapidly evolving low-level radar signatures such as quasi-linear convective system (QLCS) mesovortices and tornado debris signatures, 3) better characterization

of upper-level divergence through additional upper-level elevation cuts, 4) better sampling of the structure, magnitude, and evolution of Z_{DR} columns and K_{DP} cores, and 5) better identification of updraft characteristics such as depth and width.

4. Observations in 2023

There are a plethora of applications from both operational and research perspectives for the 2023 dataset. In the following subsections, select individual cases are discussed according to their hazard and predominant storm type. Unless otherwise noted, all dates and times are presented in UTC.

4.1. Tornadic Supercells

In 2023 there were three ATD data collection periods that focused heavily on observing tornadic supercells. Table 2 below lists the cases where tornadic supercells were the predominant hazard.

Observing Date (UTC Date)	Volume Update Time	Hazards
4/19/2023-4/20/2023*	1.5-1.8 min; 0.8-0.9 min 0.5° update	6 Tornadoes Severe Hail
5/11/2023-5/12/2023*	1.1-1.8 min; 0.7-0.9 min 0.5° update	5 Tornadoes
6/15/2023	1.1-1.7 min; 0.6-1.3 min 0.5° update	2 Tornadoes Severe Hail Wind Damage

Table 2. Case details of the tornadic supercell cases observed by ATD in 2023. Cases marked with an asterisk are summarized in a section below. Note 15 June is repeated in Table 3.

4.1.1. NOTABLE OBSERVATIONS - 19 April

ATD began operations prior to convection initiation on 19 April at about 1900 UTC. Multiple tornadic supercells were observed when ATD was operated including the pre-tornadic evolution of the Cole, OK supercell prior to 2359 UTC on 19 April.
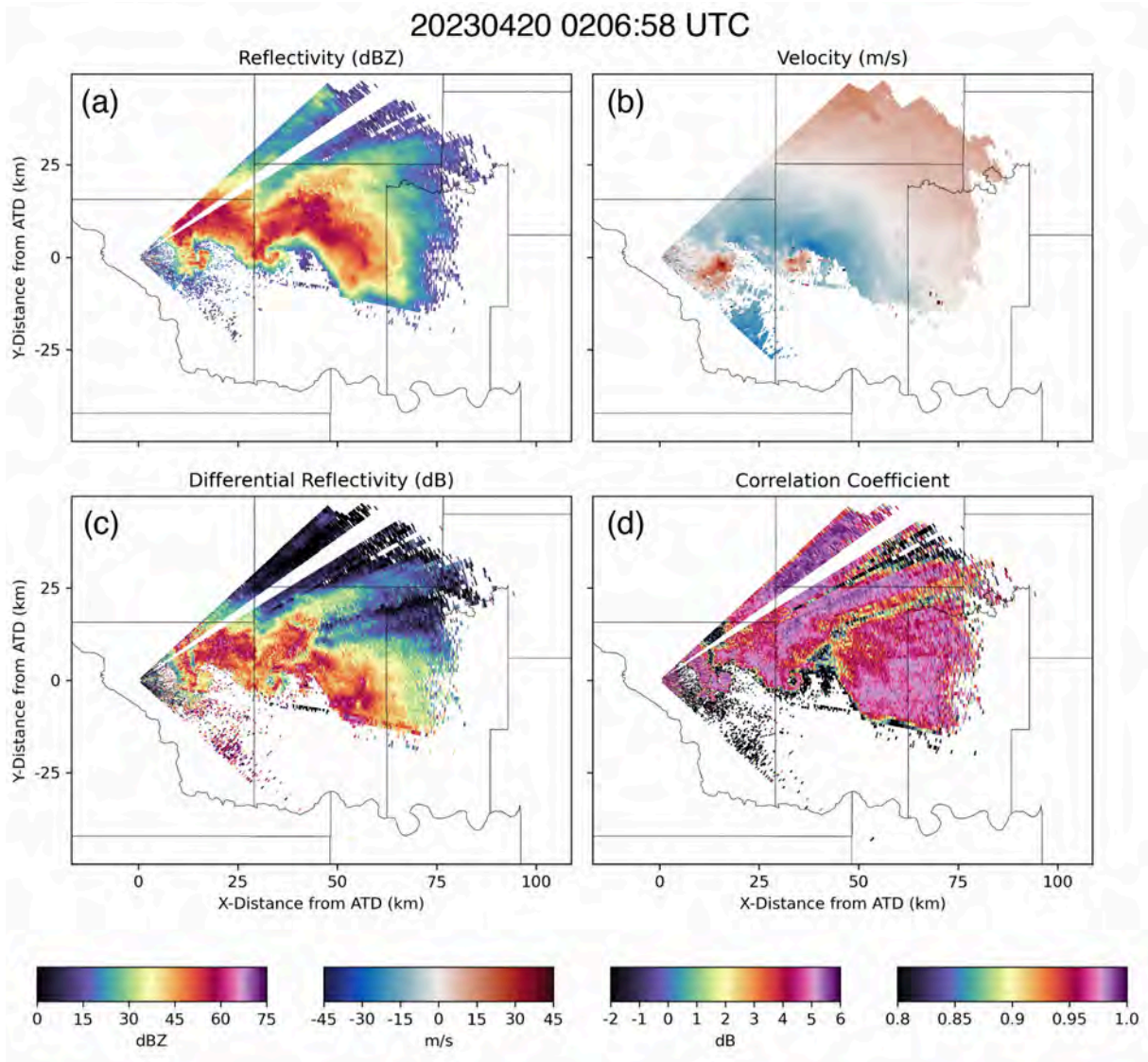
Figure 4. A 0.5° plan position indicator (PPI) of the Cole, OK supercell as it moved toward Shawnee, OK prior to merging with a second supercell on its rear flank. Reflectivity (Z_H) is shown in the top left, Doppler velocity (V_R) in the top right, Z_{DR} in the lower left, and correlation coefficient (ρ_{HV}) in the bottom right.

That particular storm passed to the south of ATD and Norman while ATD was not operating due to possible damaging reflections from a water-coated radome (see Torres and Wasielewski 2022 for further details). However, once operations resumed on 20 April 0147 UTC, a rather unique evolution occurred. The original Cole supercell, now east of Norman, continued to be observed as it produced several additional tornadoes see the eastern supercell in Fig. 4), including the Shawnee-area tornado. However, ATD began to observe a second supercell that formed directly over Norman west of the original Cole supercell and moved east. The supercell merged with the Cole storm (Fig.

5), at which point the remnant Cole mesocyclone occluded north of the new mesocyclone. Both mesocyclones produced tornadoes throughout the merger. The northern remnant mesocyclone moved west, likely due to Fujiwhara interactions between the new and old mesocyclone.
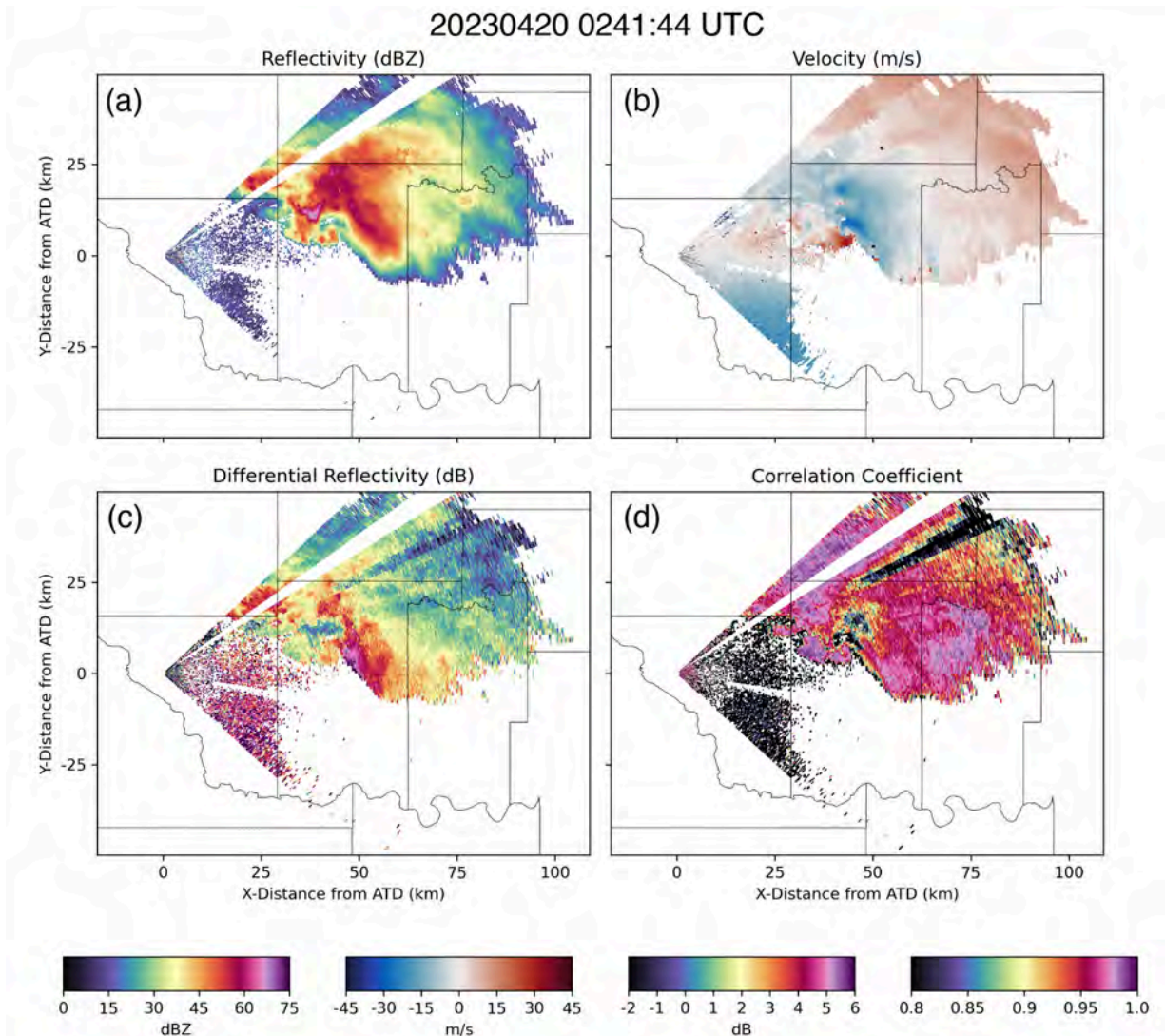
Figure 5. Same as in Fig. 4, but after the two supercells had merged.

The ATD not only observed a unique storm-scale interaction that prompted multiple tornado warnings to compensate for the deviant motion of individual tornado- and meso-cyclones, but also the supercells produced very large hail, particularly to the east of Norman along the Interstate-40 corridor. The full volume data (not shown here) well-captured the evolution of Z_{DR} and K_{DP} columns associated with the deep supercell updraft as well as low-level dual-polarization signatures associated with hail fallout (low

Z_{DR} and ρ_{HV} in Figs. 4c, 4d), TDSs (Fig. 4d), and Z_{DR} arcs related to storm-relative flow and size sorting (clear in both Figs. 4 and 5). In the current warning paradigm (i.e., stationary, storm-based warnings), the fast volumetric updates from the ATD may help operational meteorologists anticipate deviant tornado motion, hail fallout, and changes in storm structure and will be evaluated later in the HWT as well as used for research purposes.

4.1.2. NOTABLE OBSERVATIONS - 11 May

On 11 May, supercells were expected to form to the southeast of Norman. Although storms were slow to organize relative to numerical guidance, a line of supercells formed along the Interstate-44 corridor, eventually producing multiple tornadoes in the ATD viewing range. In particular, supercells producing several tornadoes to the west of Norman (e.g., Fig. 6) were observed by ATD, including the evolution of the V_R signatures, detailed high temporal resolution views of the Z_{DR} arc signatures, and hail disruptions of the Z_{DR} arcs.
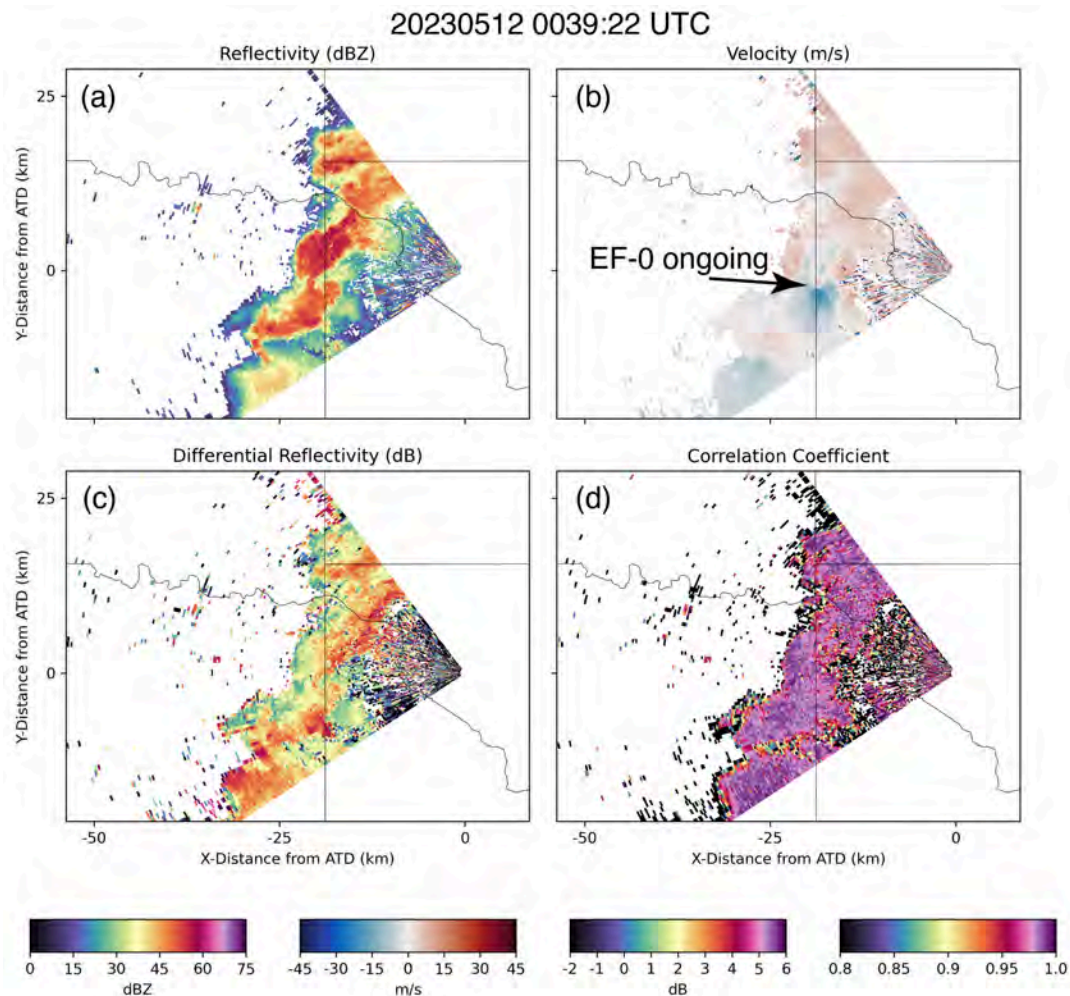
An initial dual-polarization analysis of Z_{DR} arc evolution has been performed by a NSSL Radar Research and Development Division (RRDD) summer Research Experience for Undergraduates (REU) student (Steward et al. 2023). The study found that ATD captured small, enhanced regions of Z_{DR} wrapping from the forward-flank arc into the hook echo and mesocyclone. The nearby WSR-88D, in contrast, was unable to resolve such a feature. The volumetric updates were also sufficiently fast and dense to track hail fallout that disrupted the Z_{DR} arc signature, suggesting negative buoyancy in the vicinity of the mesocyclone. Again, the WSR-88D's temporal update rate was insufficient to resolve such features.

4.2. Mesoscale Convective Systems

During 2023, nine mesoscale convective systems (MCSs) were observed by ATD, including a tornadic QLCS on 27 February 2023. During the main severe weather season (15 March to 15 June), only one MCS was observed. Typically, Oklahoma experiences a majority of its MCSs in the late spring and early summer, typically mostly in June (Haberlie and Ashley 2019). The 2023 season was no exception, but did include several mid-summer MCSs that may be considered relatively anomalous. Table 3 lists the MCS cases observed by ATD.

Observing Date(s)/Times	Volume Update Time	Hazards
2/27/2023*	2 minutes	**5 Tornadoes** **Severe Hail** **Wind Damage**
6/10/2023	1.6-1.8 minutes	**Wind Damage**
6/15/2023*	1.1-1.7 minutes	**2 Tornadoes** **Severe Hail** **Wind Damage**
6/21/2023	1.7 minutes	**No severe weather reported**
6/22/2023	20 seconds to 1.8 minutes	**Wind Damage**
6/23/2023	1.8 minutes	**Severe Hail** **Wind Damage**
7/8/2023	1.7 minutes	**No severe weather reported**
7/11/2023*	1.7 minutes	**Severe Hail** **Wind Damage**

7/21/2023	1.7 minutes	Wind Damage

Table 3. Cases that are considered MCSs are detailed. Note that 15 June is listed in Table 2 as well, as the first part of the observation period was focused on supercells and the second on a severe MCS/embedded supercells. Both are covered in this section. Cases marked with an asterisk are summarized in a section below.

4.2.1. NOTABLE OBSERVATIONS - 27 February

The 27 February QLCS tornadoes were produced by a combination of mesovortex-induced tornadoes and an embedded supercell-like structure that produced an EF2 tornado in Norman. ATD captured nearly all of the tornadoes west of Weatherford (although at a far distance), and likewise captured nearly all tornadoes west of Norman as the QLCS approached ATD. In total, thirteen tornadoes were observed throughout the event (weather.gov/oun/events-20230226).
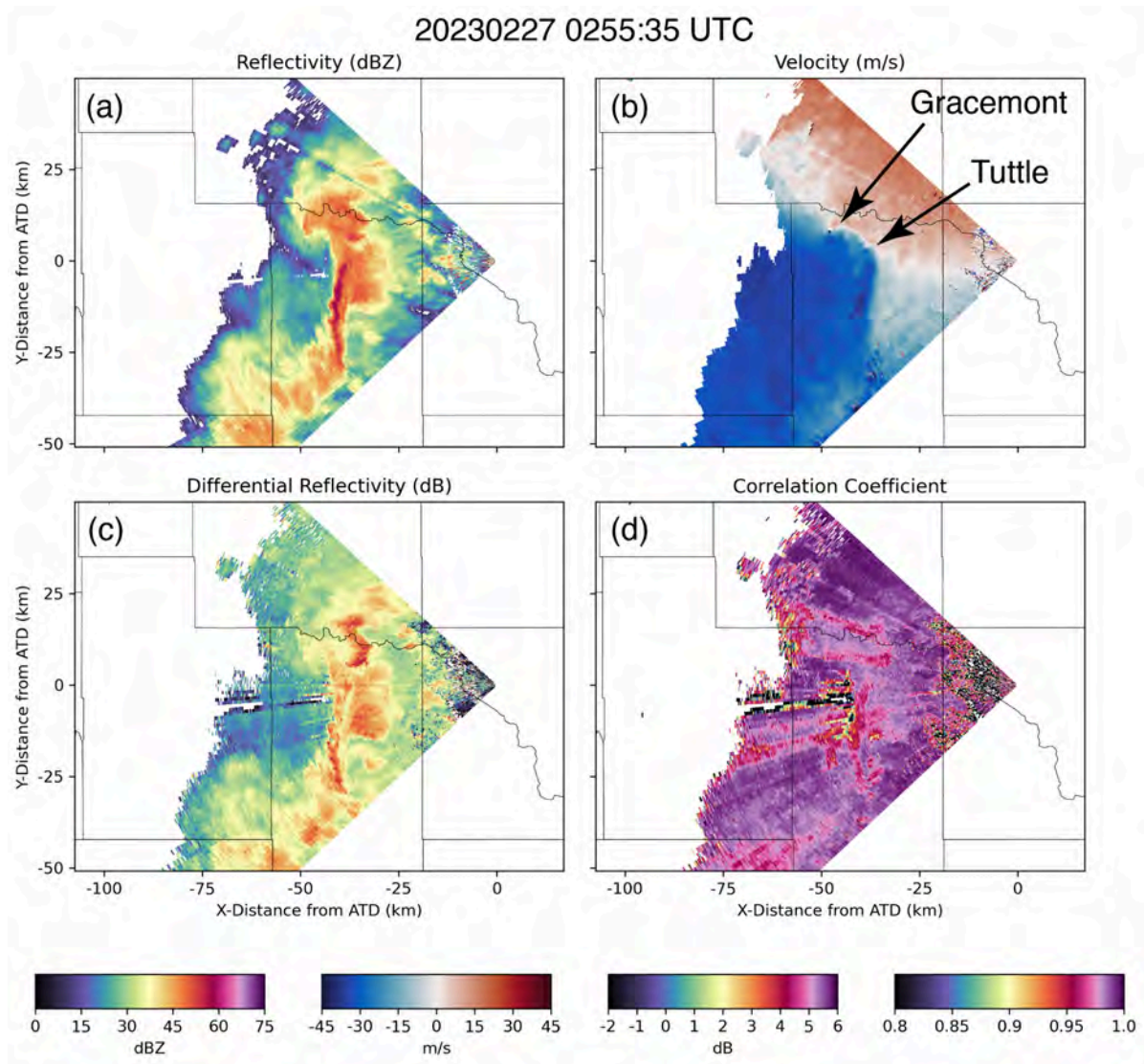
Several mesovortices were observed through the event. Figure 7 shows an intense velocity couplet at the tip of a book-end-vortex-like structure on the northern end of the convective and was associated with two EF-0 tornadoes produced to the north of Gracemont. This circulation was observed for ~30 minutes, formed on the front of the convective line before propagating north and rearward (relative to the front of the convective line), and was first observed around 0248 UTC. One of the best observed mesovortex tornadoes was the Tuttle-area EF1, which moved from southwest to northeast across the northern Grady-Canadian county line. It was associated with the Tuttle mesovortex in Fig. 7 at the intersection of the north-to-south oriented convective line and the book-end-vortex structure. The mesovortex was observed for about 20 minutes in total.
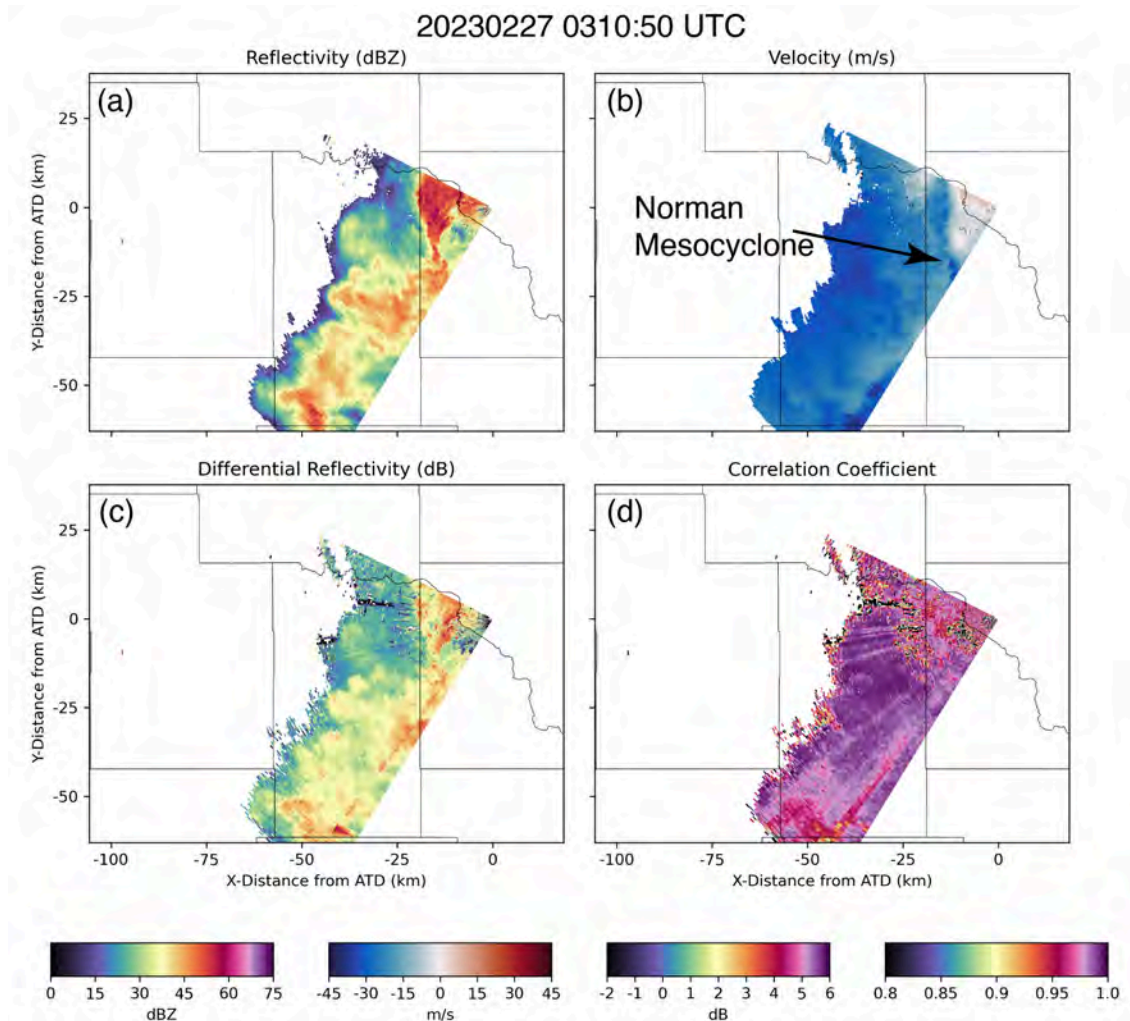
The most notable tornado of this severe weather event was the Norman EF2 tornado. Although ATD did not directly observe the Norman tornado, the near-genesis period of the tornado was observed. In Fig. 8, a supercell-like structure can be seen on the leading gust-front edge. A hook-echo structure formed on the southern portion of the supercell, coincident with the low level mesocyclone intensification and the genesis of the Norman tornado (at 0309 UTC). Interestingly, a Z_{DR}-arc structure can be seen along the eastern flank of the supercell, indicating that storm-relative flow had intensified prior to the tornado's formation Dawson et al. 2014; Segall et al. 2022) . It should be noted that additional NSSL observations exist for this case, including the mobile LIDAR vehicle, which was operated from the National Weather Center (NWC) dock area (east side of the NWC), and mobile windsondes, which were launched from just east of the NWC near the Radar Innovations Lab. The mobile windsonde profiles measured storm-relative helicity values near 1000 m^2 s^{-2} near the convective line, suggesting an environment supportive of both supercells and tornadic QLCS mesovortices.

4.2.2. NOTABLE OBSERVATIONS - 15 June

On 15 June, a severe MCS was expected to form along the western Oklahoma-Texas border in the mid-to-late afternoon along a dry line and propagate eastward through the evening. Initially, it appeared that convection initiation was on track for such a scenario. However, south of Interstate-40, a dominant supercell became the primary target of interest. Further north where supercells were originally expected, few initiation attempts materialized along the dry line until after around 16 June 0000 UTC. The southern supercell was observed by ATD from near its initiation through its maturity, which was characterized by several tornadoes, severe hail, and damaging winds. The dual-polarization signatures associated with the supercells to the southwest are shown in Fig. 9. Specifically, fine detail can be viewed in the Z_H and Z_{DR} fields, including likely areas of hail fall and a Z_{DR} arc with high Z_{DR} wrapping into the mesocyclone.
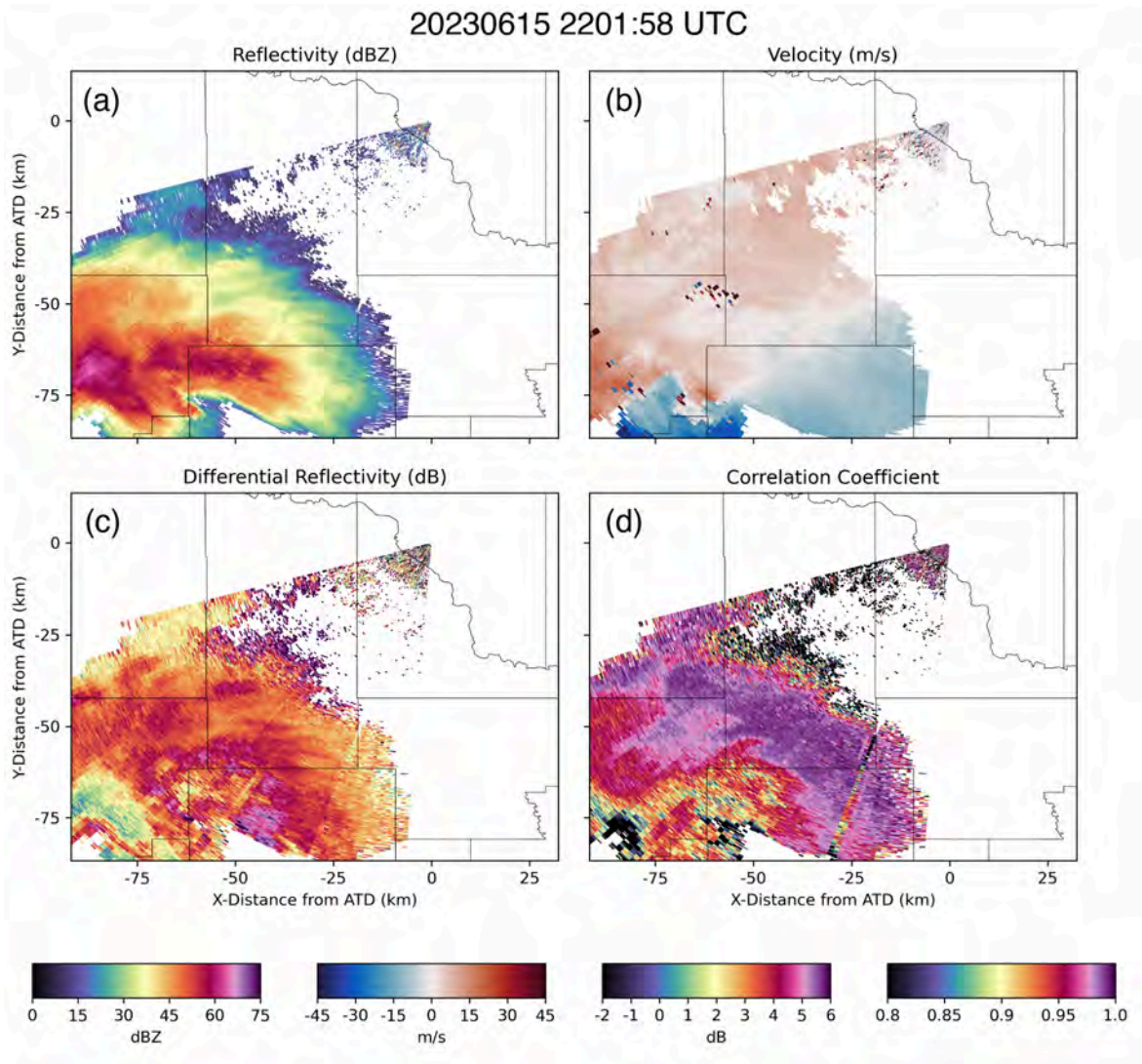
Figure 9. A supercell to the south of ATD on 15 June. Note that Z_{DR} in panel (c) is biased high by several dB. The PPI is shown at 0.5° elevation.
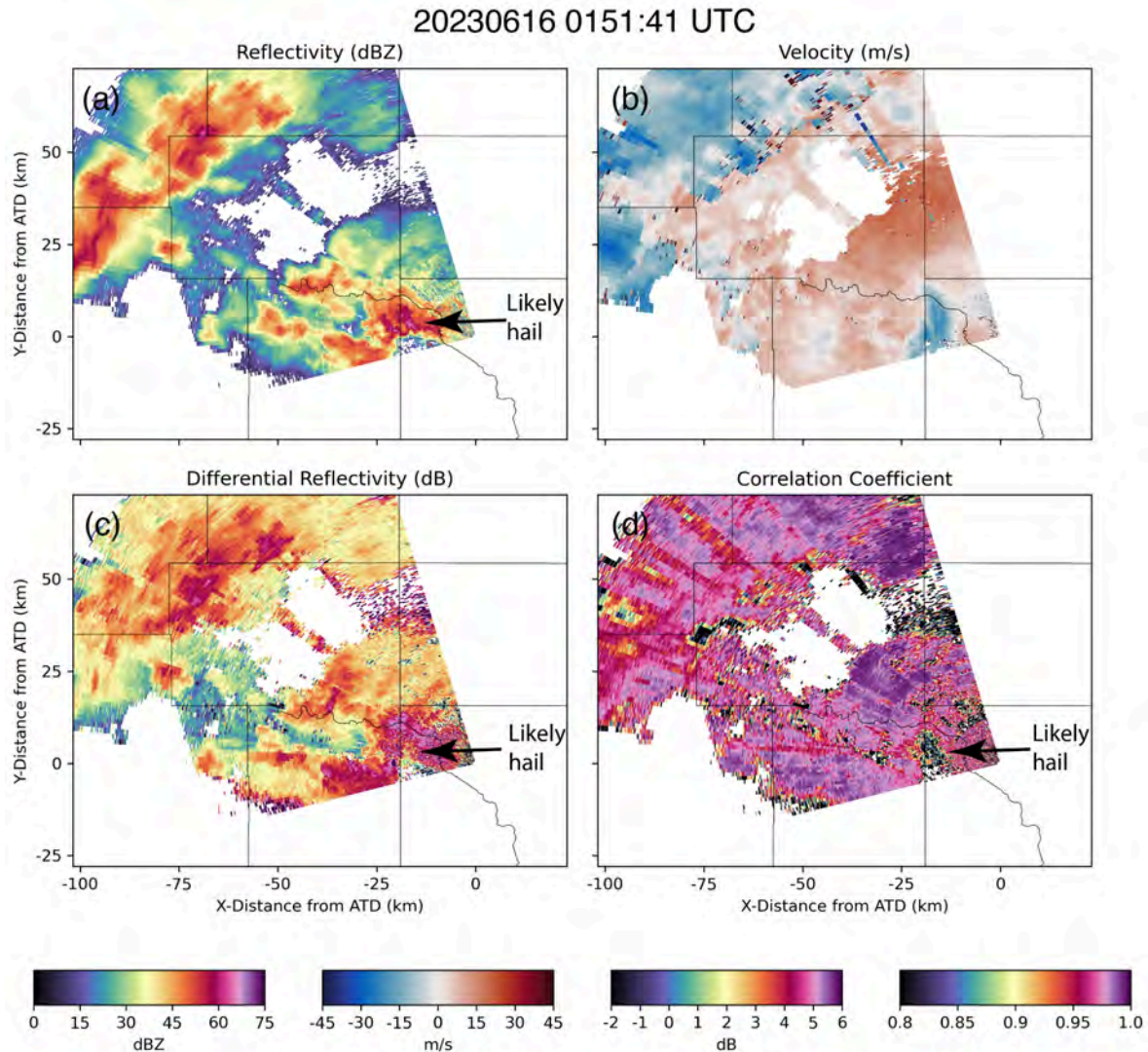
Figure 10. A 0.5° PPI from ATD at 0151 UTC showing the merged supercell/multicell convection ahead of the severe MCS approaching the Oklahoma City metro. Note that Z_{DR} is again biased high.

After observing the supercells to the southwest, ATD was turned northwest to focus on the incoming MCS and convection initiation ahead of the MCS. As the initiating supercell structures ahead of the MCS moved toward the Oklahoma City metropolitan area, the supercells (or supercell-like structures) merged into a multicell cluster which was characterized by areas of hail and severe winds (Fig. 10). Specifically, areas of high Z_H, low Z_{DR}, and low ρ_{HV} near the ATD can be seen in the leading supercell/multicell cluster. Additionally, a region of high inbound Doppler velocities can be seen, which prompted a severe thunderstorm warning by the NWS for severe winds.
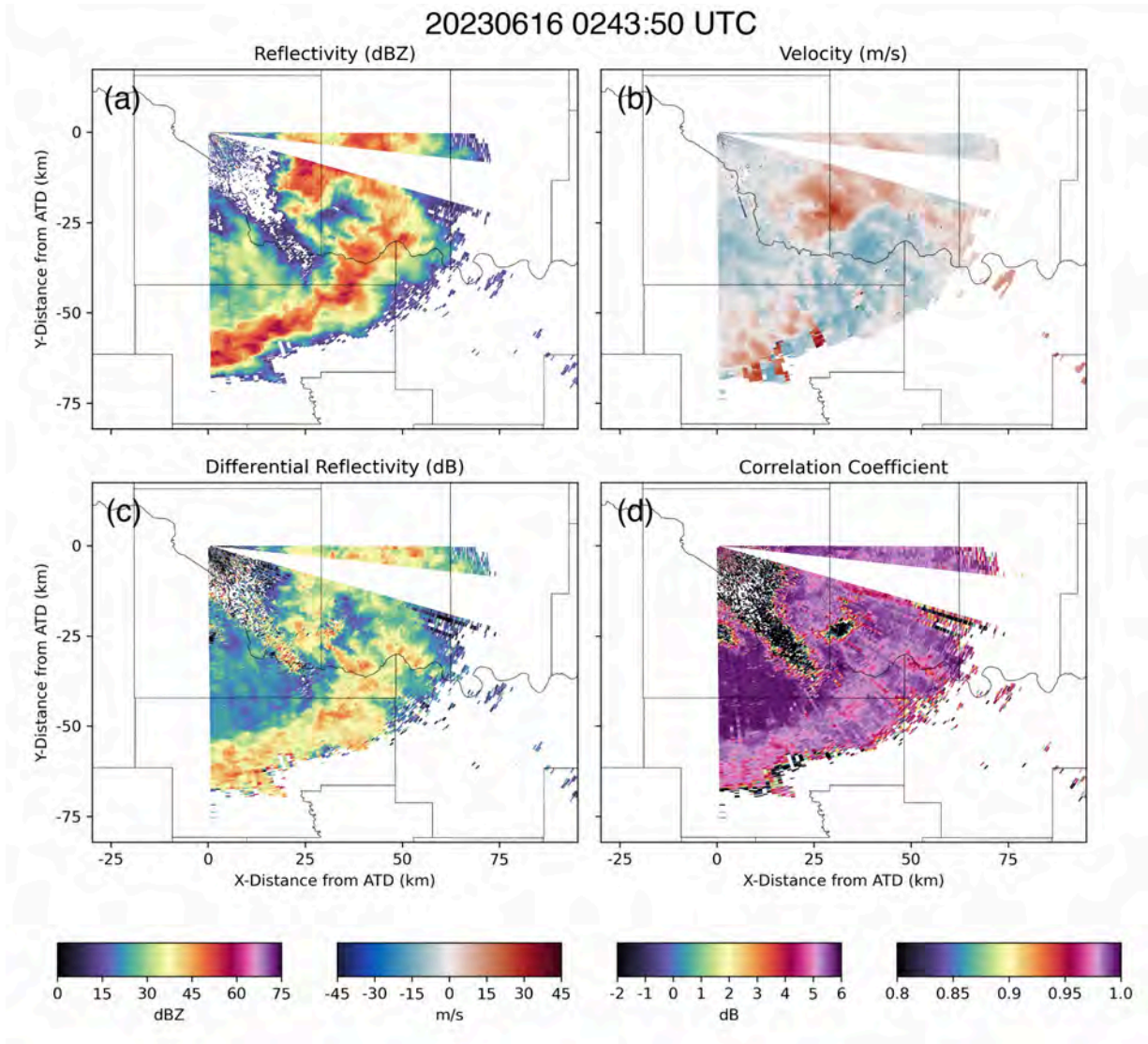
Figure 11. Observations of what appears to be a growing mesoscale convective vortex (MCV) on the northern portion of the convective line to the east of Norman. The PPI is shown at 0.5° elevation.

While the MCS passed over the ATD, operations were paused until 0237 UTC at which point ATD was turned southeast to observe the convective line and a northern mesoscale convective vortex (MCV; Fig. 11). The supercell/multicell cluster grew upscale into a convective line with a northern-end MCV. The previous MCS seen in Fig. 10 weakened rapidly and its gust front became decoupled from the convection. The MCV was characterized by broad convergence in the V_R field, and was observed for about a ten-minute period. The remainder of operations were split between the dying MCS and weakening cold pool to the north and the MCS to the southeast.

4.2.3. NOTABLE OBSERVATIONS - 11 July

A late-night MCS was observed on 11 July that prompted severe thunderstorm and flash flood warnings across the Oklahoma metropolitan area. The evolution of this particular event was not that of a classic MCS, but of slowly organizing multicell convection that eventually merged into a large cold pool driven system. Multiple gust fronts produced by collapsing convection were observed both prior to and within the MCS, including those in Figs. 12 and 13. In general, regions of convection were observed through the evening to form, mature, and dissipate, similar to the conceptual model of multicell upscale growth.
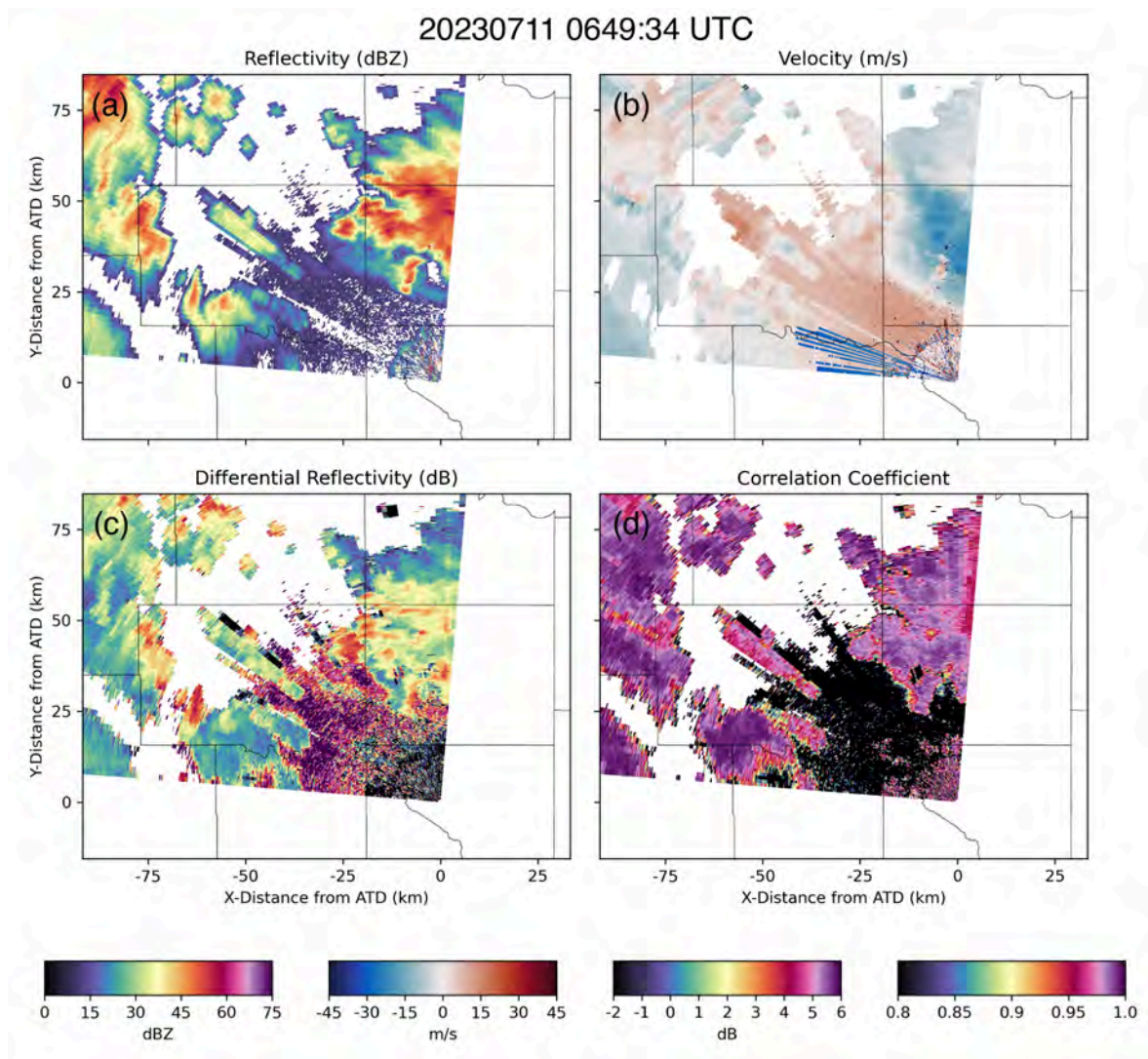
Figure 12. A 0.5° PPI showing the upscale growth of convection ahead of a severe MCS. The storm on the eastern edge of the sector prompted flash flood warnings in Edmond/OKC and a severe thunderstorm warning due to the surging gust front, visible in the V_R in (b).

Within the MCS (Fig. 13), a particularly intense area of convection was observed. Eventually, a substantial cold pool formed and propagated to the east toward the Oklahoma City metro. At this time, the previous cold pool associated with the Oklahoma City storm (Fig. 12) had been in place across the western portion of the metropolitan area. As the cold pool in Fig. 13 interacted with the OKC-storm cold pool, several waves were observed, likely indicative of gravity waves atop the stable cold pool. Convection initiation was broadly observed by ATD. Slowly over the next hour, convective coverage increased to the north and west of ATD. In summary, this was an interesting mesoscale event that likely combines multiple conceptual models of upscale growth (e.g., McAnelly et al. 1997).
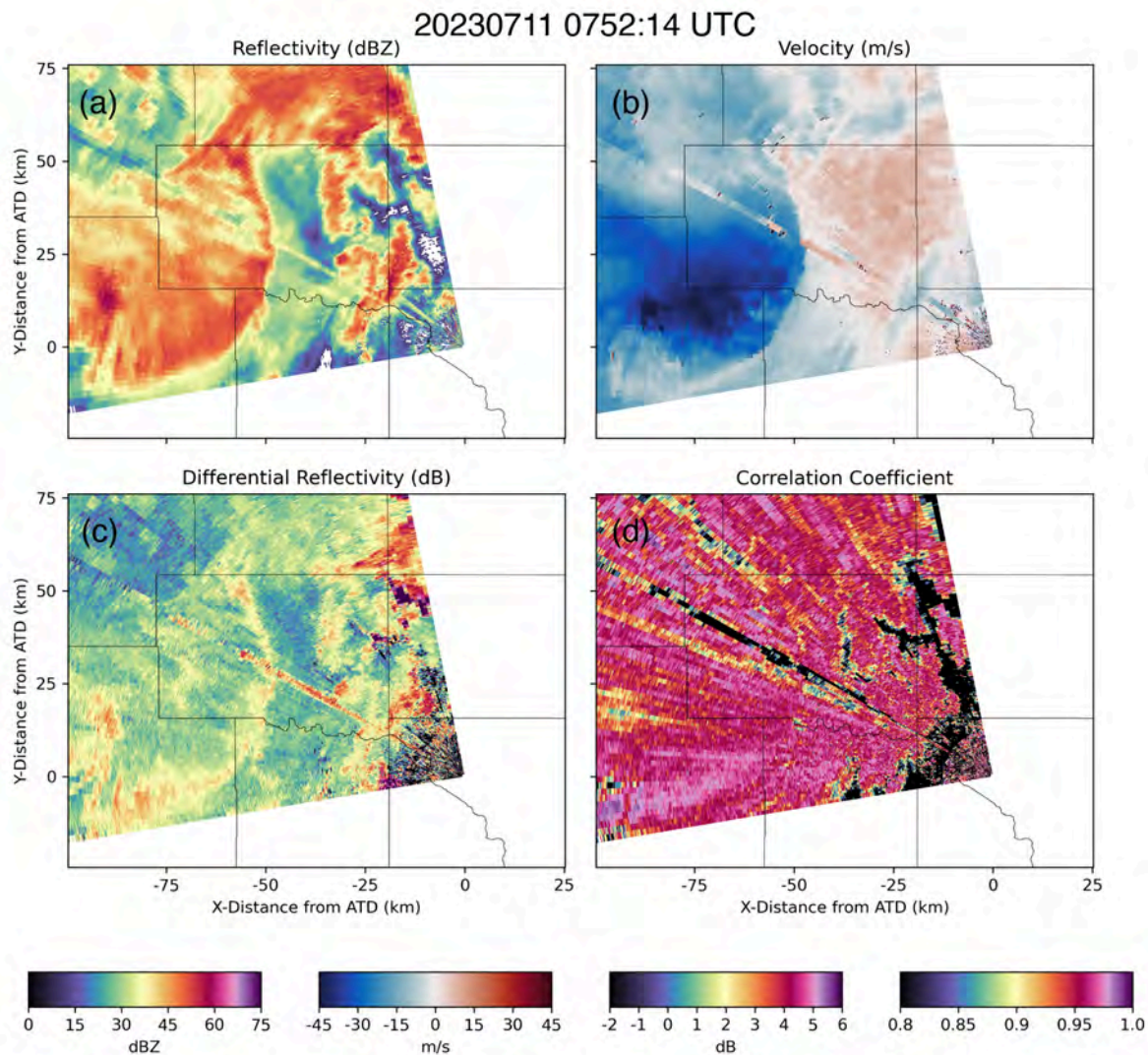
Figure 13. A bowing segment that was propagating toward ATD prior to shutdown on 11 July. The PPI is shown at 0.5° elevation.

4.3. Severe Multicell Convection

An assortment of cases (Table 4) were focused on severe convection without tornadic potential. Severe hail was the predominant hazard associated with this subset of cases. Here, the 10 April case is summarized, which saw 2.0" (5.1 cm) hail reports near Kingfisher, OK.

Observing Date(s)/Times	Volume Update Time	Hazards
3/16/2023	1.5-2 minutes	Severe hail
3/23/2023-3/24/2023	1.5-1.8 minutes	Severe Hail
4/10/2023-4/11/2023*	1.8 minutes	Severe Hail
5/6/2023-5/7/2023	1.7 minutes	Severe Hail Severe Winds
5/12/2023-5/13/2023	1.1-1.8 minutes	Severe Hail
6/14/2023	1.3-1.7 minutes	Severe Hail
8/26/2023-8/27/2023	1.3 minutes	Severe Hail Severe Winds
9/19/2023	1.3-1.5 minutes	Severe Hail
9/24/2023	1.5 minutes	Severe Hail

Table 4. A summary of cases encompassing the severe multicell cases collected by ATD. Cases marked with an asterisk are summarized in a section below.

4.3.1. NOTABLE OBSERVATIONS - 10 April

Severe hail-producing thunderstorms were observed under an anomalous flow pattern where storm motions from north to south were observed. Storm motions were quite slow, but the environment was favorable for intense updrafts capable of severe hail. Eight ≥1.5" (3.8 cm) hail reports were recorded in central Oklahoma, largely near Kingfisher, OK. Relatively small hail-core footprints were observed by ATD and the central Oklahoma WSR-88Ds. For example, in Fig. 14 high Z_H cores co-located with local Z_{DR} minima can be seen on the northwest side of the Kingfisher-area storm. Note that the PPI in Fig. 14 was observed coinciding with a 2" hail report in Okarche. The local Z_{DR} minima are quite small and are difficult to observe in corresponding WSR-88D data (not shown).
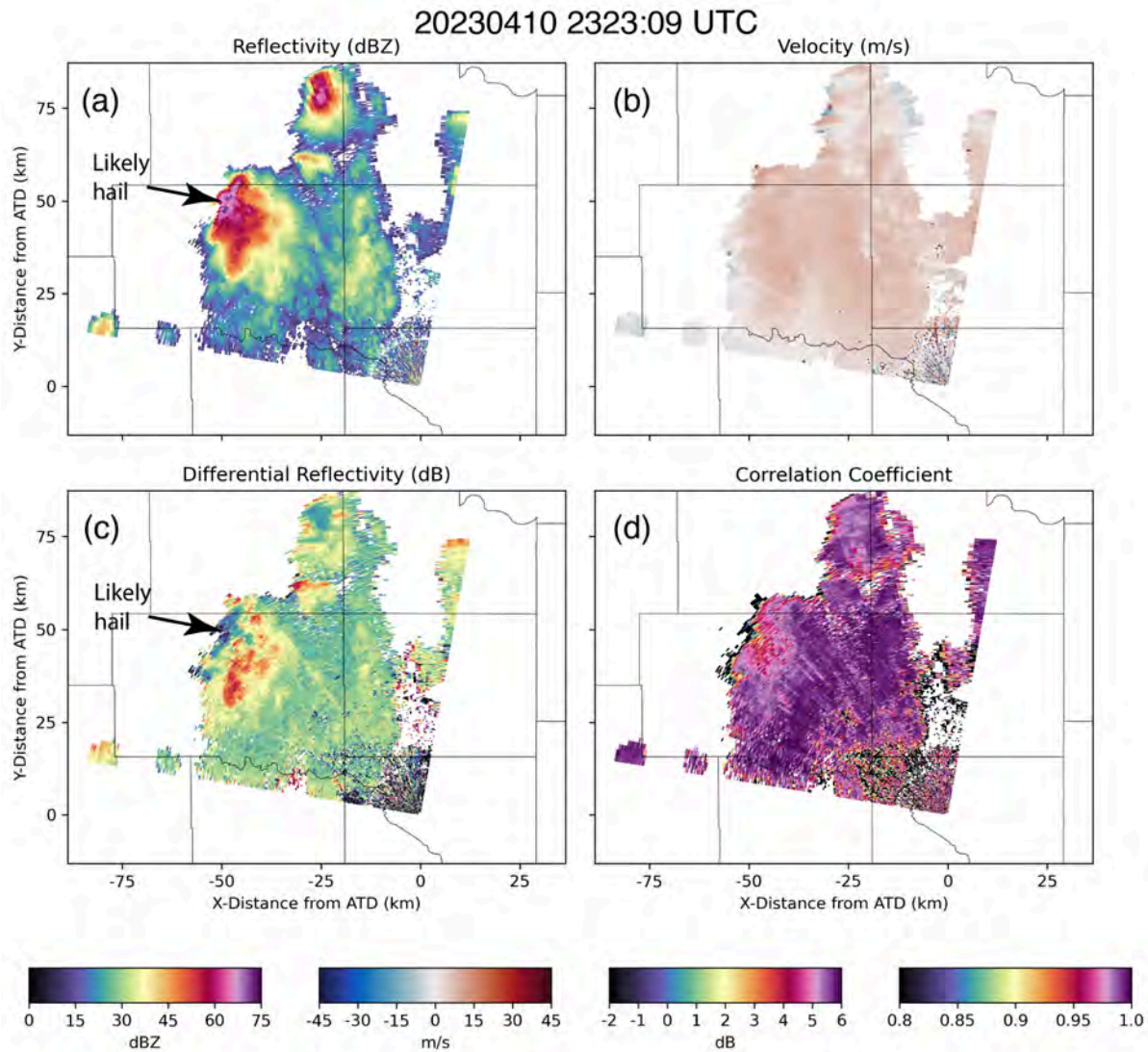
Figure 14. Severe multi-cell storms on 10 April with the most prominent being near Kingfisher, OK (the southwestern storm in the figure). The PPI is shown at 0.5° elevation.

Here, the spatial data quality afforded by the advanced signal processing techniques and PAR is apparent. Due to electronic beam steering, the ability to collect rapid-update volumes with dense vertical sampling was also well-tested in this case. Figure 15 shows a pseudo-range height indicator (pseudo-RHI) through the hail core in Fig. 14. KOUN, the co-located (with ATD) NSSL research WSR-88D, was operated in VCP 212. A pseudo-RHI was constructed along an azimuth of 315° from an ATD volume and a KOUN volume. Clearly, the ATD's denser vertical sampling (with elevation angles added between the typical VCP 212 elevation angles) is superior in resolving:

  1) the full vertical extent and details of the deep convection including the depth of the ≥60-dBZ echo and the 30-dBZ echo,

2) size sorting signatures in the low levels associated with high Z_{DR} near 60-km range indicative of large drops and/or melting hail, and

3) hail at approximately 70-km range associated with Z_{DR} near 0 dB and Z_H above 60 dBZ.

Such features are much more difficult to discern from WSR-88D (KOUN) data.
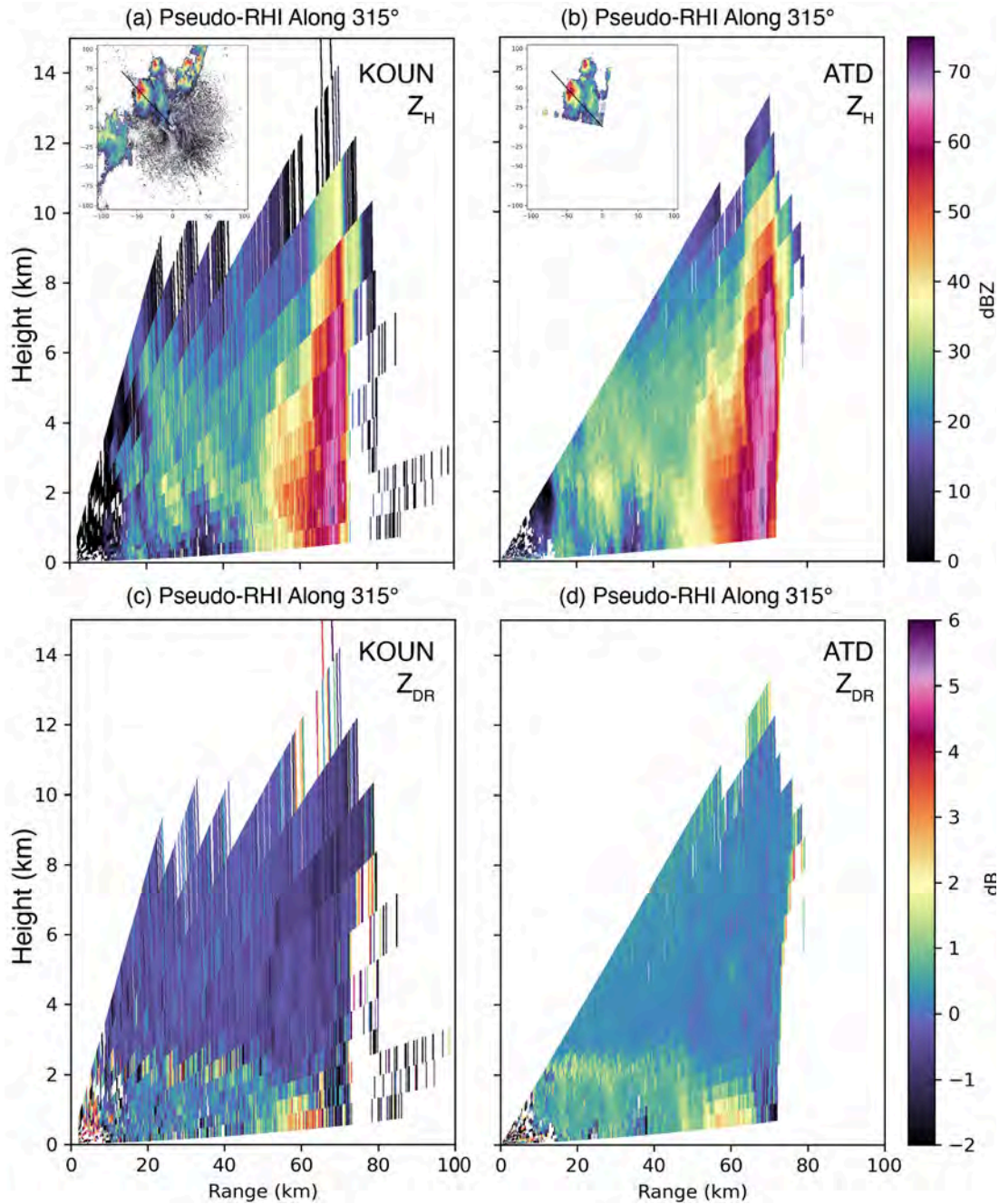
Figure 15. A comparison of KOUN (left column) and ATD (right column) reconstructed or pseudo-RHIs through the same storm of focus in Fig. 14. For reference, the insets in the top row show the location of

Similarly in Fig. 16, a hail core of small spatial extent can be seen after the storm had moved south. As in the former paragraphs, the Z_{DR} data quality in particular shows a narrow region of decreased Z_{DR} on the northwest side of the storm.
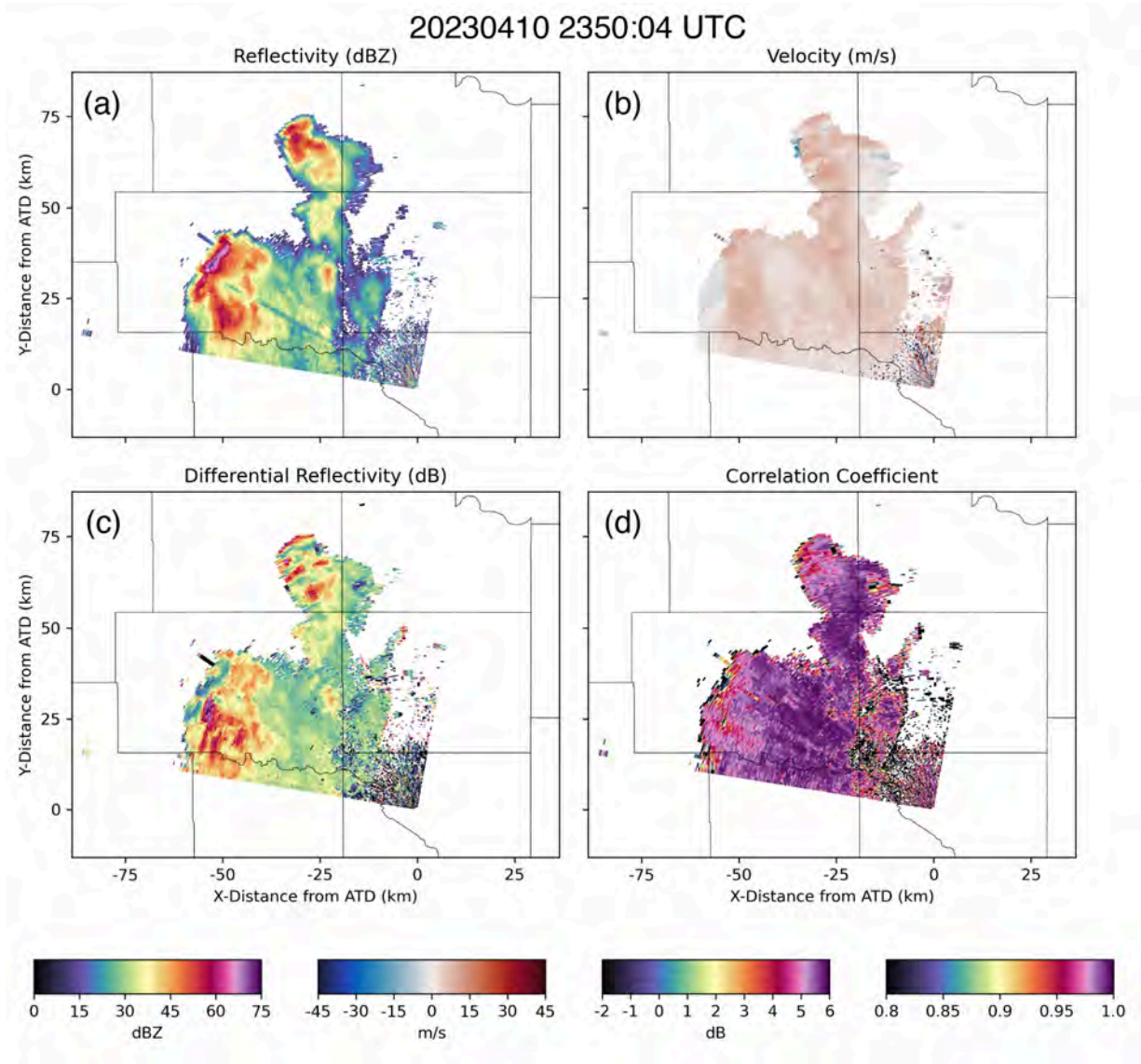
Figure 16. A 0.5° PPI of the Kingfisher-area storm as it produced a second 2" (5.1 cm) hail report.

4.4. Non-Severe Multicell Convection

Although severe weather was a large focus of the 2023 data collection efforts, the ATD was leveraged to collect datasets focused on radar-based applications such as quantitative precipitation estimation (QPE) in non-severe settings. Primarily, the datasets described in Table 5 encompass data collection during non-severe single- and multi-cell convection and stratiform precipitation events. The cases vary in range from the ATD, which may be used to examine the utility of rapid-update dual-polarization volumes as a function of range. Below, the 28 April case is briefly described.

Observing Date(s)/Times	Volume Update Time	Description
2/15/2023	<2 minutes	VCP testing in non-severe convection
2/22/2023	<2 minutes	VCP testing in non-severe convection
3/2/2023	U	U
3/30/2023	2 minutes	VCP and radar testing
4/5/2023	2 minutes	Cold frontal convection and clear air
4/24/2023	1.7 minutes	QPE in light convective and stratiform rain
4/25/2023	1.7 minutes	QPE in light convective and stratiform rain
4/26/2023	1.3-1.7 minutes	QPE in light convective and stratiform rain
4/28/2023*	1.3 minutes	QPE in light convective and stratiform rain
5/4/2023	N/A	N/A
5/10/2023	N/A	Non-severe hail
5/13/2023	N/A	Multicell convection and flash flooding
5/23/2023	1.3 minutes	QPE in light convective and stratiform rain
5/24/2023	1.3 minutes	QPE in light convective and stratiform rain

6/2/2023	1.3 minutes	Multicell convection
6/7/2023	1.4 minutes	QPE in light convective and stratiform rain
6/12/2023	1.4 minutes	QPE in light convective and stratiform rain
7/15/2023	1.2-1.7 minutes	Weakening convection
8/7/2023	N/A	Testing post exciter replacement

Table 5. A summary of the non-severe multicell convection cases collected by ATD. Cases marked with an asterisk are summarized in a section below. A "N/A" indicates that the dataset was collected for demonstration purposes, largely for engineering testing or operator training.

4.4.1. NOTABLE OBSERVATIONS - 28 April

On 28 April, an area of stratiform precipitation moved from the northwest to the southeast toward ATD. Within the precipitation shield, narrow enhanced precipitation bands (perhaps associated with weak convection) were observed, similar to those in Fig. 17. The primary reason for collecting data was to directly compare QPE data between the ATD and operational WSR-88D (using KOUN). For example, it is hypothesized that the enhanced data quality afforded by ATD may yield better QPE retrievals, particularly those QPE methods leveraging dual-polarization moments in the retrieval process. In Fig. 17, the dual-polarization structure of the bands of enhanced precipitation and the lighter rain regions suggest complexity in terms of the microphysical structure inferred from dual-polarization data. For example, the heaviest band in the Z_H field is offset to the north of two extensive, but narrow bands of high Z_{DR}. In most studies, such structure would typically imply the presence of size sorting. It is unclear in this case, however, the cause of such changes in dual-polarization structures. This particular case, in addition to the wide variety of cases discussed here, will be leveraged in an ongoing Ph.D. project at NSSL.
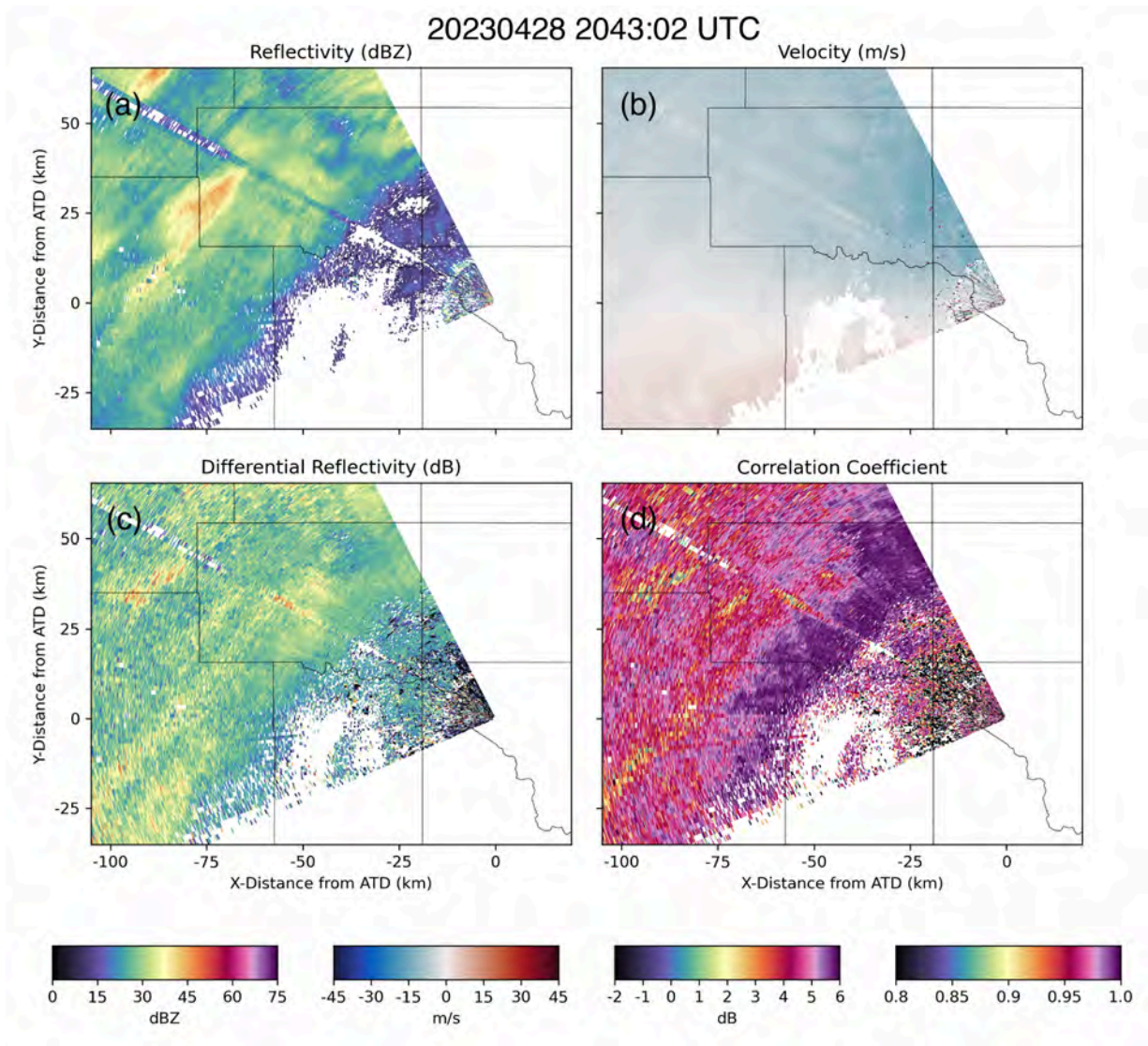
Figure 17. An example 0.5° PPI of nearing stratiform precipitation to the west of ATD on 28 April. The linear "streak" of low Z_H, Z_{DR}, and ρ_{HV} are due to beam blockage from nearby buildings.

4.5. Downbursts

The early part of June yielded several wet downburst cases. Special VCPs were designed to focus specifically on downburst signatures with elevation angles prioritized in the mid-levels of the atmosphere to document the evolution of, for example, mid-level K_{DP} cores. We focus here on summarizing the 6 June case, as a unique combination of PPI-based and RHI-based volumes were leveraged. Table 6 lists the cases classified as downburst cases.

Observing Date(s)/Times	Volume Update Time	Description
6/1/2023	1.4 minutes	Non-severe downbursts and downburst VCP testing
6/5/2023	1.4 minutes	Non-severe downburst collection
6/6/2023*	20 s to 1.4 minutes	Non-severe downbursts with RHI scans that observed multiple downburst signatures
9/5/2023-9/6/2023	1.5 minutes	Severe downbursts near ATD

Table 6. A summary of the downburst cases collected by ATD in 2023. Cases marked with an asterisk are summarized in a section below.

4.5.1. NOTABLE OBSERVATIONS - 6 June

On 6 June, convection initiation began in the early- to mid-afternoon. With wind shear being rather weak, single-cell to multicell convection was observed across central Oklahoma. Updrafts were observed to mature quickly and collapse, sometimes yielding weak downburst signatures (i.e., the change in Doppler velocities as a function of range was small, on the order of 5 m s^{-1}) at 0.5° elevation observations. Figure 18 shows an example from the portion of PPI-based data collection prior to RHI collection when the ATD was being operated with a HWT experiment in mind. The convection denoted in the figure was observed to initiate, mature, and weaken within about a 30-minute period at which point additional convection formed on the storm's outflow. Little low-level divergence was observed in this particular storm. The dual-polarization signatures suggested that initially drop size distributions were shifted toward larger drops and transitioned to distributions with smaller droplets near cell dissipation.

After a temporary hardware issue at 1950 UTC, technicians were able to restore ATD operations at 2040 UTC at which point it collected RHI data for a 1.5-hr period. The RHI sector was changed depending on the target of interest, but a particularly mature storm southwest of El Reno, OK (RHI azimuth about 309°) yielded several features of

note. In Fig. 19, the growth of the updraft at 62-km range is depicted with mid-level divergence seen in the V_R field. Z_H in the mid-level core reached 55+ dBZ and a Z_{DR} column can be seen extending above the melting level (approximately 3.5-km altitude). K_{DP} values were not substantial at this time. However, about fifteen minutes later in Fig. 20, the mature updraft stage of this particular storm can be seen. Mid-level divergence was replaced by substantial mid-level convergence at this time. Z_H values above 60 dBZ in regions of low Z_{DR} above the melting level suggest the storm was producing hail aloft. Below the mid-level Z_H core, regions of high Z_{DR} and high K_{DP} (i.e., K_{DP} core) can be observed below the region of mid-level convergence. After this time, several core collapses were observed (not shown) in the plane of the RHI before the storm began dissipating. Weak outflow was observed in the low elevations of the RHIs coincident with the core collapses.
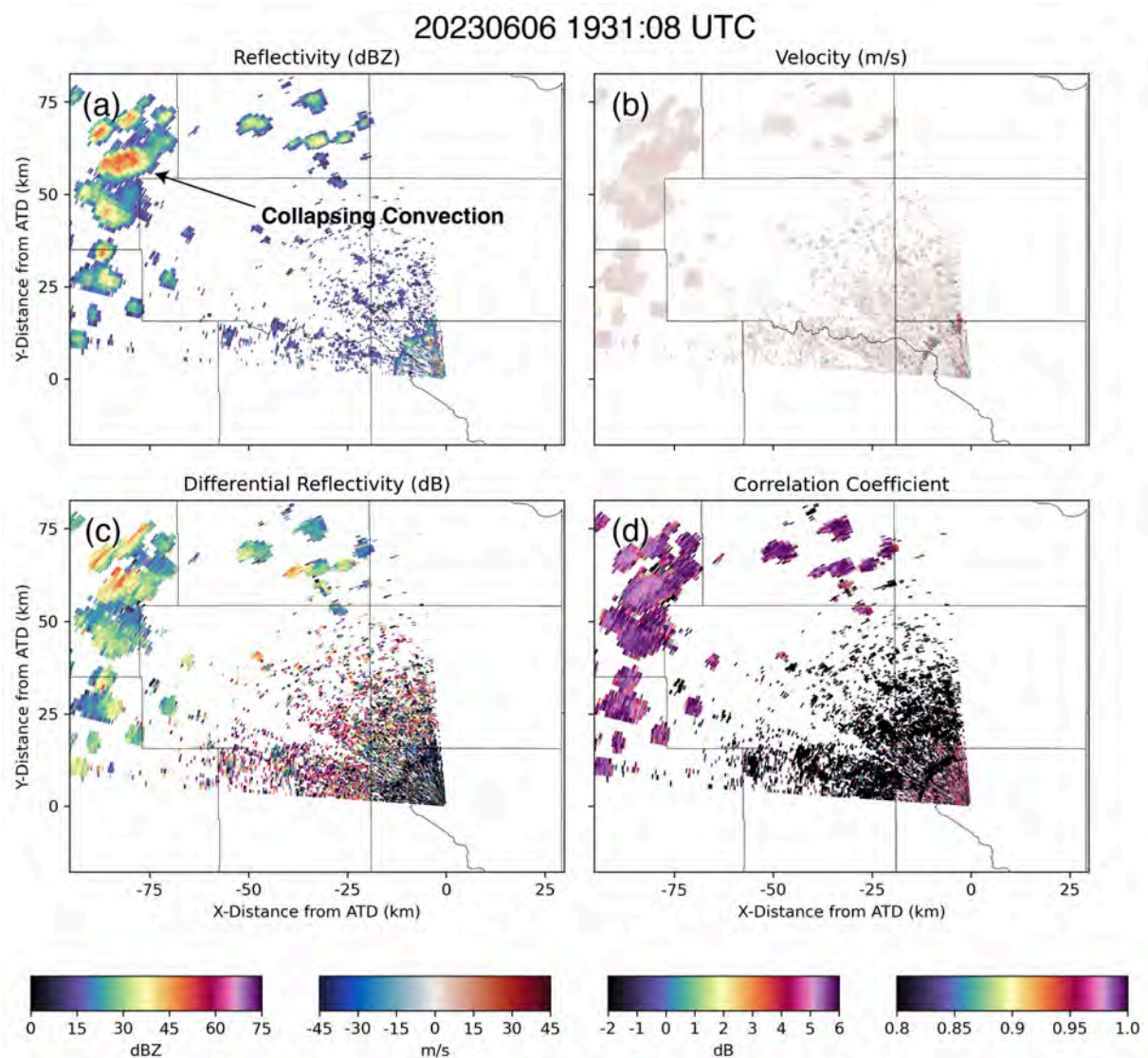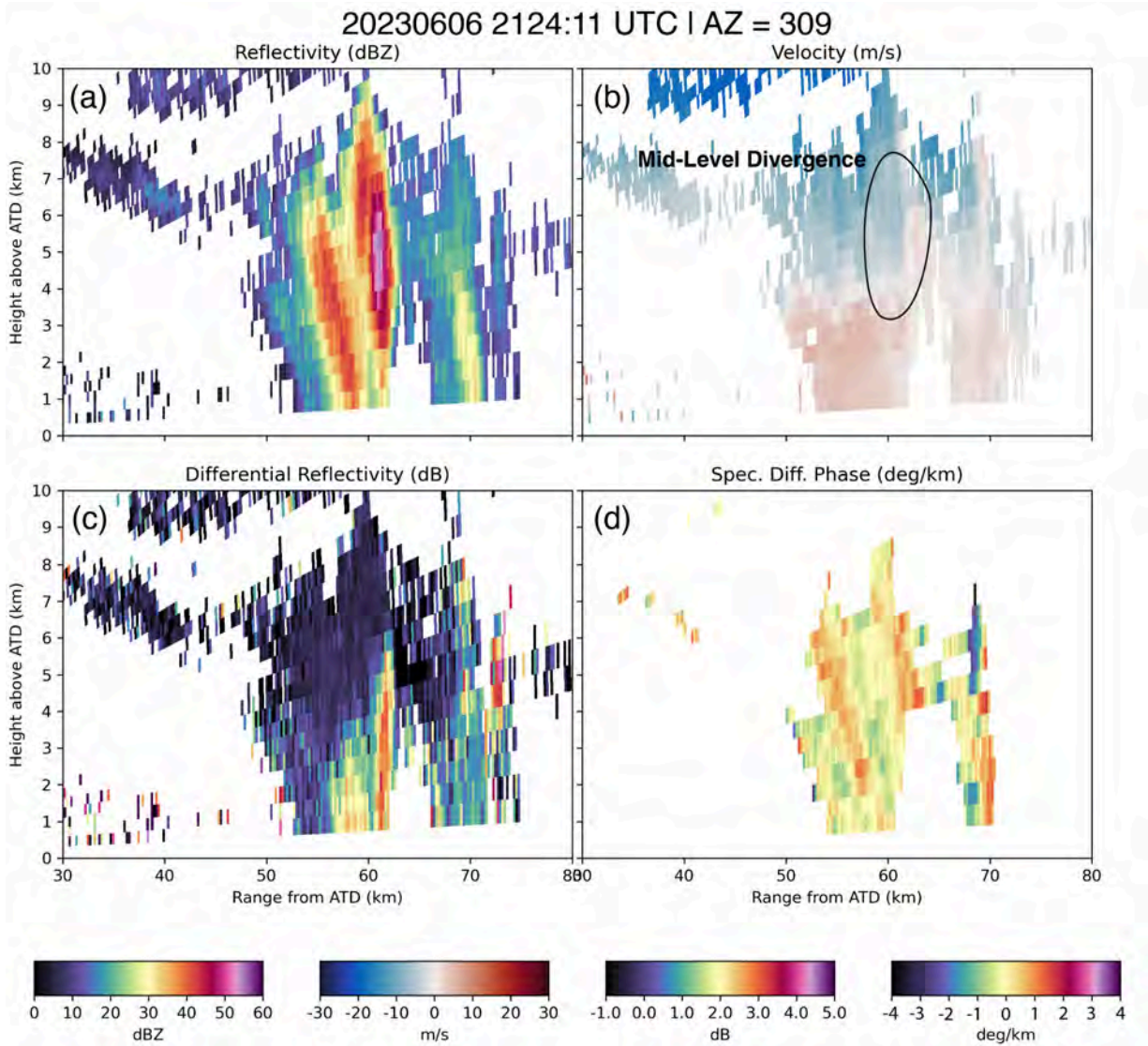
Figure 19. A growing updraft observed by ATD in RHI mode (note the data captured were true RHIs, not pseudo-RHIs). An area of mid-level divergence is denoted in the V_R panel.
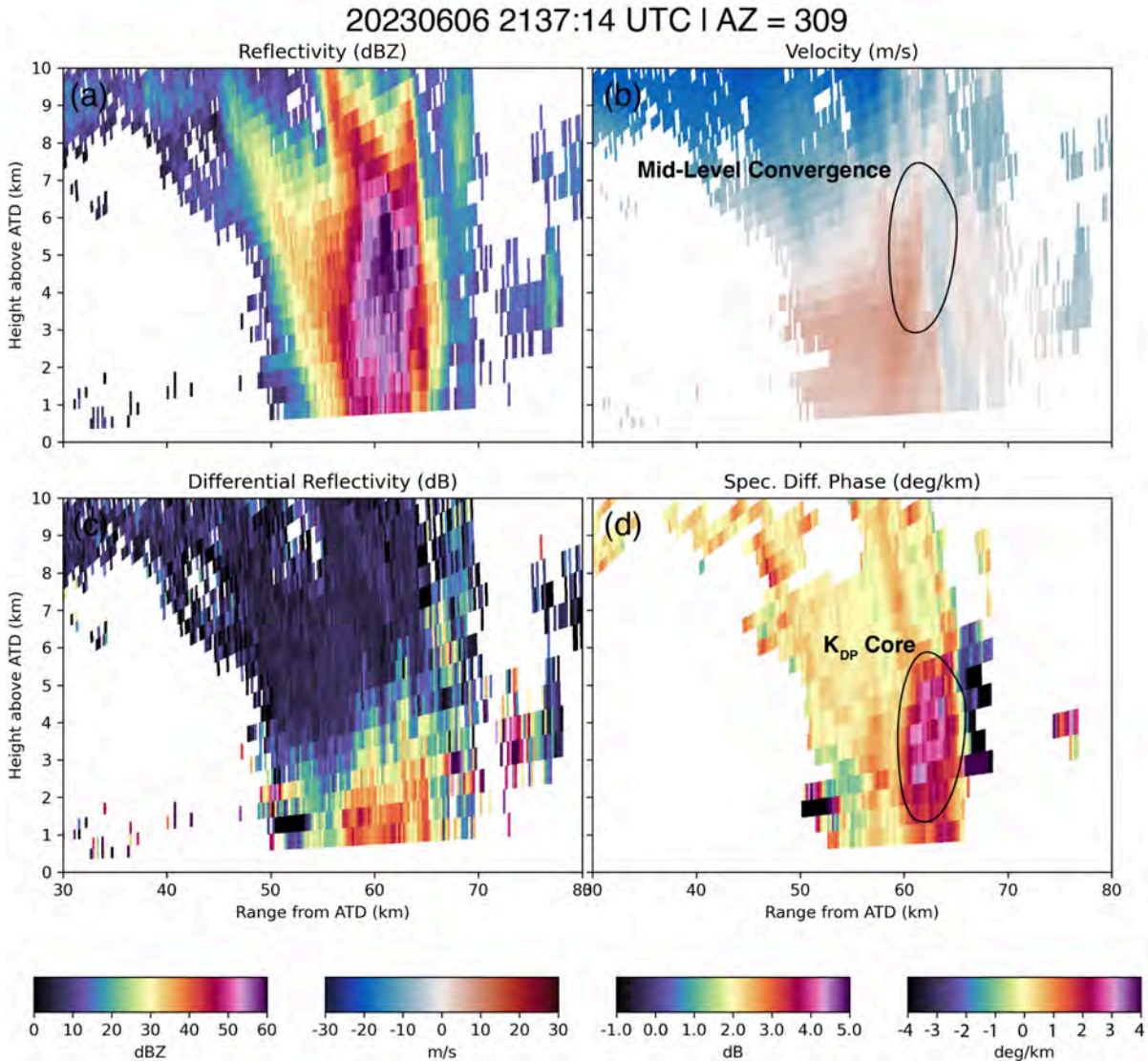
Figure 20. A mature updraft observed by ATD in RHI mode prior to the updraft collapse. An area of mid-level convergence is denoted in the V_R panel.

4.6. Winter Weather

In 2023, two winter weather events were observed by ATD (Table 7). The first was a rain-to-snow transition event on 24 January, and observations were limited due to possible damaging reflections from a water- and/or snow-coated radome. On 30 January, a dry sleet event occurred, which allowed for a longer observation period. A summary of the latter is given below.

Observing Date(s)/Times	Volume Update Time	Description
1/24/2023	2.5 minutes	Observed a rain-to-snow transition event
1/30/2023*	35 s to 2.5 minutes	Observed a sleet event and performed RHIs

Table 7. A summary of winter weather events captured by the ATD. Cases marked with an asterisk are summarized in a section below.

4.6.1. NOTABLE OBSERVATIONS - 30 January

On 30 January, operations observed a sleet event in central and southern Oklahoma. Sleet was generally expected given that the 1200 UTC sounding from the NWS Norman weather forecasting office showed an elevated warm layer from about 1-3 km above the surface and a significant freezing layer below 1 km (between -10 and 0°C). Convective sleet showers were observed through the duration of the event (e.g., Fig. 21). Z_H values near the surface often approached 50 to 55 dBZ in the cores of the most intense echoes (Fig. 21).

One of the primary tasks of the ATD was to examine the benefits of the ~2.5-min volumetric update afforded by the specially designed winter weather VCP versus the conventional WSR-88D scanning strategy (about 6 minutes). Relative to the operational VCP, the ATD winter weather VCP was designed with vertical density in mind, and included significantly more elevation angles than the WSR-88D strategy. Figure 22 shows pseudo-RHIs through a convective sleet shower at 30-km range in each RHI from both the ATD and KTLX. Although viewing angle and RHI azimuth selection may account for some differences, the vertical depth of the convective echo shows up more clearly in ATD data than data from KTLX. It is anticipated that the advection of the shower out of the plane of the pseudo-RHI in KTLX may account for a lack of significant echo aloft, but still emphasizes the benefit of rapid update and high-density elevation VCPs achievable with PAR observations.

In addition to resolving the convective structures in individual sleet showers, the high-density elevation cuts also allow for easier identification of the melting level (Fig. 22). Although not directly comparable to one another due to differences in point angles, the melting level is more difficult to identify in KTLX data than in ATD data. The increase in ρ_{HV} below the melting level in the sub-freezing layer below 1 km is also more detectable in ATD data, likely due to the addition of a 0.75° elevation angle between the typical ~0.5° and ~0.9° (1.0° for the ATD in this particular case) elevation cuts typical of WSR-88Ds.
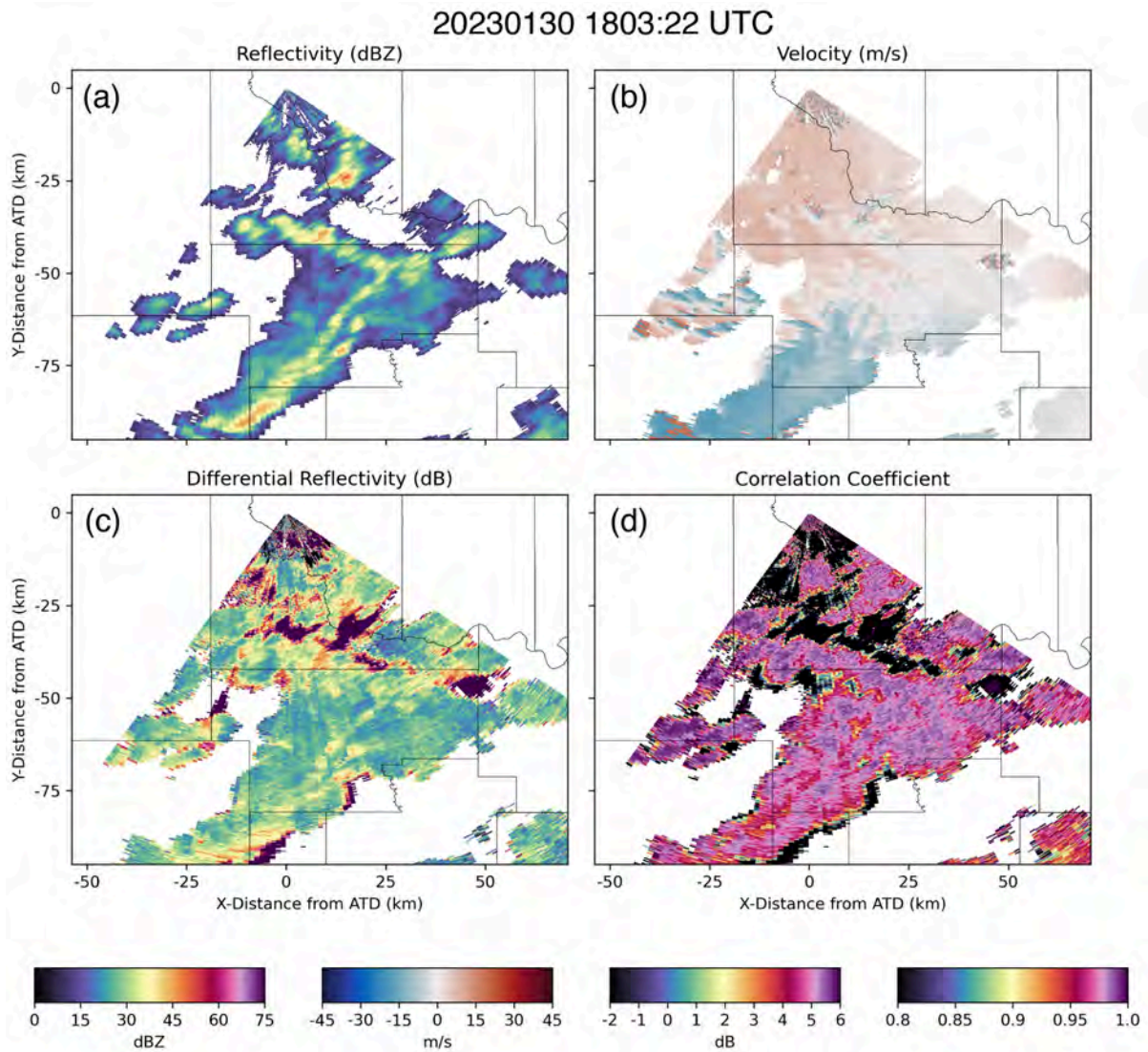
Figure 21. A 0.5° PPI from ATD showing convective sleet showers south of ATD.
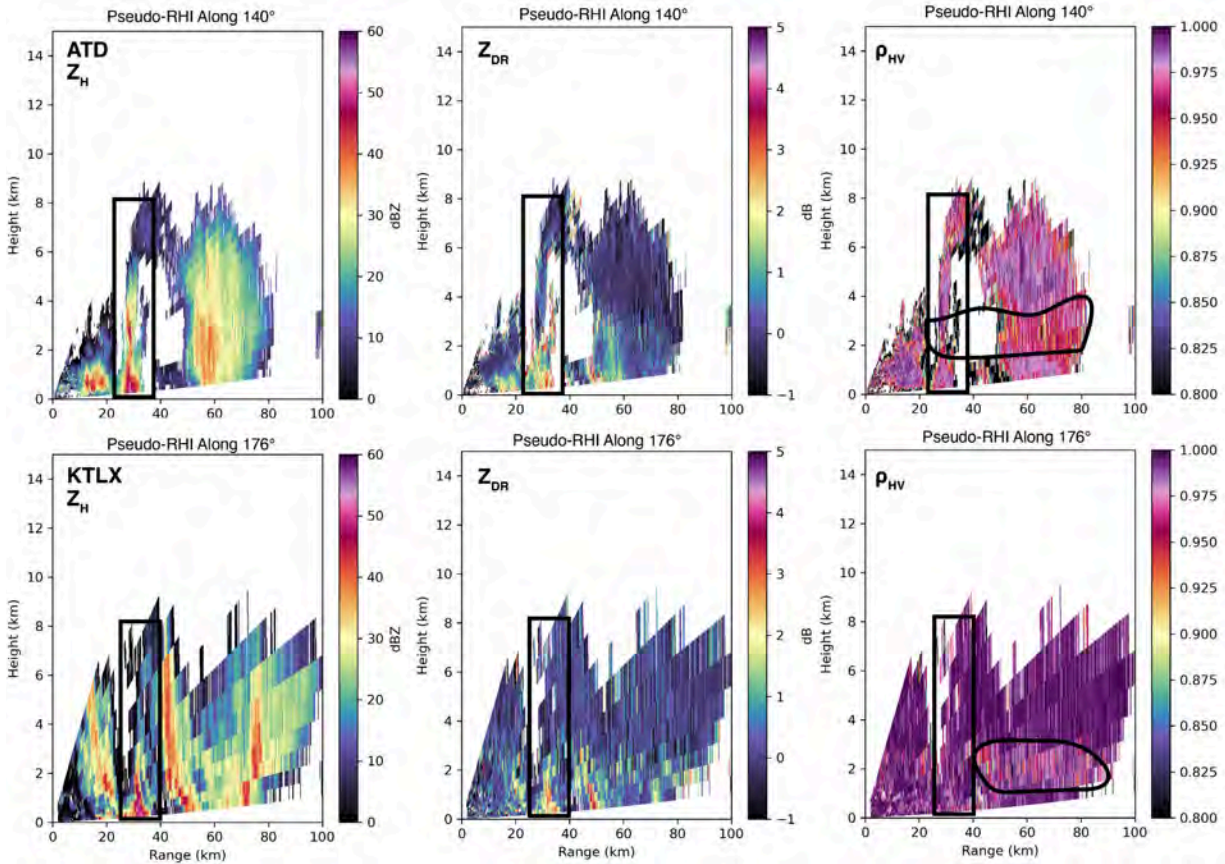
Figure 22. Pseudo-RHIs taken through a convective sleet shower at 30-km range from both the ATD and KTLX. The storm of interest is outlined in each panel by the black rectangle. The black curves in the ρ_{HV} point out the elevated melting region identified by reduced correlation values. Both volumes began at approximately 1806 UTC.

4.7. Clear Air and Engineering Testing

In addition to the pure meteorological datasets collected by ATD described in the above sections, ATD data collection periods to support engineering testing and to examine clear-air echoes in fire weather, for example, were also performed. Self-consistency testing was performed to support the validation of ATD dual-polarization calibration. In short, stratiform rain encompassing a significant portion of the 90° ATD sector was targeted. Low-level elevation cut volume scans were collected with each volume being rotated +/- 0, 10, 20, or 30° from a central pointing angle (e.g., the antenna position was changed from 0 to -10° to +10 and back to 0° and so forth, all relative to the original pointing angle of the ATD antenna). The preliminary results of the self-consistency data collection supported that the ATD dual-polarization data are well calibrated (not shown).

Fire weather data were also collected to 1) examine the benefits of rapid update and polarimetric PAR observations in observing smoke plumes and 2) examine the detectability of smoke echoes by ATD. In short, significant fires were able to be well-observed by ATD, particularly those <100-km range. Further work is needed to examine the operational benefit of PAR observations in fire weather. A summary of clear air and engineering tests is shown in Table 8.

Observing Date(s)/Times	Volume Update Time	Description
3/6/2023	N/A	Data collection used for engineering testing
3/9/2023	N/A	Data collection used for self-consistency testing
3/13/2023	N/A	Data collection used for self-consistency testing
3/22/2023	N/A	Testing clear air scans and detectability of clear air echoes with varying pulses per radial
3/31/2023	2.5 minutes	Observing smoke plumes
4/4/2023	N/A	Observing smoke plumes and dryline
5/3/2023	N/A	Clear air testing
5/19/2023	N/A	Monitoring for landspouts
5/22/2023	N/A	Short data collection to examine 5G interference with varying degrees of interference filters
5/25/2023	N/A	Data collection used for self-consistency testing and could be used for QPE
8/9/2023	N/A	Examining ATD sensitivity

Table 8. The data collection periods by ATD examining clear-air returns and engineering tests.

5. Summary and Discussion

In this report, notable observations from the NSSL ATD have been documented. The ATD observed numerous supercell, multi-cell, and single-cell storms that produced tornadoes, hail, severe winds, and flooding in 2023. In addition to severe convective weather, a plethora of non-severe observations were captured that ranged from downbursts to winter weather to engineering evaluation and testing. Specialized scanning strategies that targeted dense vertical observations of the former phenomena were developed to evaluate the benefits of PAR beyond solely rapid updates. Operating in pencil beam mode and mimicking one side of a four-panel PAR, the ATD was able to collect more rapid update volumes (typically <2 minutes) while also providing denser vertical elevation samples relative to what WSR-88D systems are capable of providing.

In Section 3, three primary objectives were discussed for the 2023 season. In brief, they were to 1) leverage ATD to collect novel PAR observations to observe severe weather for research and operational evaluation, 2) evaluate the effectiveness of denser vertical sampling while exceeding the update time of WSR-88Ds, and 3) collect novel use cases for assessment in the HWT. As documented in Section 4, 57 use cases were collected that spanned severe and non-severe weather events, well achieving the first objective. Due to the use of specialized scanning strategies that included denser elevation angles than typically achieved by WSR-88D and other conventional mechanical scanning radars (in an effort to satisfy objective 2), research and operational sampling strategies for severe and non-severe weather were aligned. Upon review of the cases that were collected, at least 13 cases were identified as being suitable for potential future use in the HWT, satisfying the third objective.

5.1. Spatiotemporal Benefits of PAR

In the 2000s and 2010s, the NSSL SPY-1A PAR demonstrated many of the benefits of rapid-update radar data, particularly for forecasters. It is not surprising that more rapid updates lead to better observations of rapidly-evolving phenomena such as tornadoes. The WSR-88Ds often leverage the Supplemental Adaptive Intra-Volume Low-Level Scan (SAILS) technique to increase the temporal visits at 0.5° elevation, which has led to operational warning improvements (Kingfield and French 2022). However, Kingfield and French (2022) explicitly note that the use of SAILS leads to a total decrease of mid-level elevation scans per hour, which can make resolving mid and upper-level dual-polarization signatures difficult.

Figure 15 in particular highlights the differences in ATD PAR observations versus WSR-88D observations in terms of vertical sampling (Objective 2). The structure of the Kingfisher hail storm is much better resolved by ATD in Fig. 15, and was sampled in

under two minutes compared to ~5 minutes by KOUN. Alford et al. (2023), Reinhart et al. (2023), and Schuur et al. (2023) likewise examined the Kingfisher storm in addition to other ATD cases and found similar results. Similarly, a study undertaken by a summer REU student evaluated the spatiotemporal benefits of PAR by examining the 11 May 2023 tornadic supercells west of the Oklahoma City area (Steward et al. 2023). Specifically, the project was aimed at examining Z_{DR}-arc signatures in ATD data compared to a nearby WSR-88D. Steward et al. (2023) found that the evolution of the Z_{DR}-arc structures was superior in ATD data due to the temporal update rate increase. However, the spatial benefits were not directly related to the vertical sampling of the Z_{DR} arc itself, which is known to be a relatively shallow dual-polarization signature. Instead, the descent of a hail core above the Z_{DR} arc was well-tracked in ATD data and ultimately led to a disruption of the low-level Z_{DR} arc (Objectives 1 and 2). When comparing the data to the WSR-88D, the less frequent temporal updates coupled with more sparse elevation angles aloft led to almost no ability to track the hail-core descent over time.

Work from Kuster et al. (2019, 2021, 2023) has also shown the utility of pre-cursor dual-polarization signatures in operational settings with particular emphasis on Z_{DR} columns and K_{DP} cores, similar to those seen in Figs. 15 and 20, respectively. For example, Z_{DR} columns are often used to evaluate the strength of an updraft, and K_{DP} cores can be used to anticipate downbursts. Their use in anticipating tornadoes, however, is less clear. Kuster et al. (2023) showed evidence that tornadic QLCS mesovortices were often associated with the development of a mid-level K_{DP} core that developed prior to the near-surface mesovortex. Mesovortex development is also associated with a drop in near-surface K_{DP} according to Kuster et al. (2023). However, much of the knowledge of the evolution of dual-polarization signatures near tornadic and non-tornadic mesovortices comes from WSR-88D observations. Initial evaluation of ATD data during the 27 February 2023 QLCS (Figs. 7 and 8) by Kuster et al. (2023) and Alford and Kuster (2024) indicates that the vertical evolution of dual-polarization data is much better captured by the ATD. In particular, ATD allows a more comprehensive examination of dual-polarization signatures in both vertical space and in time, including the vertical evolution of Z_{DR} and K_{DP} to diagnose radar-inferred microphysical and thermodynamic processes (Objectives 1 and 2). Work to extend Alford and Kuster (2024) is ongoing.

5.2. ATD Data Quality

A notable characteristic of ATD data is the quality of its dual-polarization data compared to WSR-88D dual-polarization data. As described by Boettcher et al. (2023), ATD data are significantly less noisy (low spatial variance) than WSR-88D data. Z_{DR} data are particularly less noisy from the ATD than from comparable WSR-88D data. For example, the Z_{DR} arcs associated with the tornadic supercell storms in Figs. 4-6 are

particularly clear (Objective 1). Steward et al. (2023) specifically noted the clarity of the Z_{DR} arc during the 11 May 2023 supercells west of Oklahoma City that is seen in Fig. 6. A narrow extension of the Z_{DR} arc was shown to wrap into the mesocyclone in the case, which was a feature almost indiscernible in WSR-88D data.

The lower variance of the ATD data results from an effective increase in sampling per radar range gate. The ATD uses pulse compression and has a native range spacing of 37.5 m. To more directly compare ATD data to WSR-88D data, six range gates are averaged to achieve a 225 m range gate (close to the 250 m gate spacing of the WSR-88Ds). In effect, the range data are oversampled by a factor of six, yielding a factor of six more samples per 225 m range gate than what would otherwise be achieved per radar pulse. This technique is not exclusive to PAR and can be theoretically applied to most (if not all) weather radars. However, it is possible that the technique provides the added benefit to dual-polarization data quality via PAR in both stationary and rotating concepts. Specifically, there are no beam smearing effects in a stationary PAR concept. In a rotating PAR concept, beam smearing can be minimized by steering the radar beam to consistent locations as the antenna rotates to collect radar pulses in approximately the same direction per azimuth collected. Work to evaluate the measurement quality of the ATD in quantitative applications (e.g., precipitation estimation) and other spatiotemporal benefits afforded by PAR is ongoing.

5.3. Hazardous Weather Testbed

Operational evaluation of PAR data is a key component to determining how it may be useful to an operational meteorologist (Objective 3). In the 2010s, the Phased Array Radar Innovative Sensing Experiment (PARISE) was developed to examine the benefits of rapid-update PAR data collected by the single-polarization NSSL SPY-1A PAR. Bowden and Heinselman (2016) and Wilson et al. (2017) showed that the perception and understanding of radar data were better when a forecaster received 1-minute updates versus forecasters who received 5-minute updates. They noted that forecasters were able to use the higher temporal updates to identify and track trends in severe convection that likely led to more timely and accurate warnings. However, dual-polarization radar data were unavailable with the SPY-1A.

PARISE was conducted in the HWT, which is a joint testbed between NSSL and the NWS. Beginning in 2024, HWT experiments will be conducted using ATD data to evaluate use of polarimetric PAR data by operational meteorologists. Many of the use cases described in this report are candidates for the HWT experiments. For use in the HWT, cases will need to meet at least the following minimum working criteria that will be refined over time:

1) Radar observations of severe and/or non-severe storms exist over at least a 30-min period and are mostly continuous with no significant gaps in data (e.g., an error in the system that required restarting the radar).
2) Continuous radar observations exist for at least a 20-min period prior to any storm reports.
3) No significant data problems exist that would distract an operational meteorologist or other end user.

In total, we expect that at least ten of the thirteen use cases previously mentioned will have the criteria above and will be potentially used in the HWT beginning in July 2024 (Objectives 1 and 3) and beyond. Additional datasets collected in 2024 (and beyond) will likewise be considered depending on the experimental setup and targeted point of evaluation.

5.4. Future Operations

2023 was a very successful year of ATD data collection, yielding numerous operational and research use cases. As discussed earlier, the ATD operated in stationary, pencil-beam mode and mimicked one side of a four-panel PAR during 2023 data collection efforts. Additional capabilities are being developed and implemented on the ATD including rotating PAR, beam spoiling, and adaptive scanning. Such techniques as reviewed in Section 2b will afford even greater temporal-update improvements and will also yield additional flexibility in approaching scanning techniques. For example, in a 1-minute window, it may be possible to collect rapid update volumes typical of what an operational meteorologist might use in addition to collecting range-height indicators through a target of interest or collecting a focused volume on a significant storm. For 2024 specifically, 1-minute stationary volumes with a pencil beam will be of primary focus. To achieve near 1-minute updates VCPs will be developed to distribute elevation angles ideally to examine both low-level hazards and mid/upper-level pre-cursor signatures. Through coordination and collaboration between the engineering and meteorological teams that jointly operate the ATD, spoiled transmit beam testing will proceed and rotating operations in pencil-beam mode will also be examined where appropriate.

6. Acknowledgements

to thank Thea Sandmæl and Dr. Ted Mansell for their comments that helped to improve the quality of this report.

7. List of Acronyms

- ART Advanced Radar Techniques
- ATD Advanced Technology Demonstrator
- ρ_{HV} Correlation Coefficient
- ϕ_{DP} Differential Phase
- HWT Hazardous Weather Testbed
- K_{DP} Specific Differential Phase
- MCS Mesoscale Convective System
- MCV Mesoscale Convective Vortex
- NOAA National Oceanic and Atmospheric Administration
- NSSL National Severe Storms Laboratory
- NWC National Weather Center
- NWS National Weather Service
- OAR Oceanic and Atmospheric Research
- PAMST Phased Array Radar and Meteorological Analysis Studies Team
- PAR Phased Array Radar
- PARISE Phased Array Radar Innovative Sensing Experiment
- PPI Plan Positioning Indicator
- QLCS Quasi Linear Convective System
- QPE Quantitative Precipitation Estimation
- RED Radar Engineering and Development
- REU Research Experience for Undergraduates
- RHI Range Height Indicator
- RRDD Radar Research Development Division
- SAILS Supplemental Adaptive Intra‑Volume Low‑Level Scan
- TDS Tornado Debris Signature
- WSR-88D Weather Surveillance Radar 1988 Doppler
- VCP Volume Coverage Pattern
- Z Reflectivity
- Z_{DR} Differential Reflectivity

8. References

Alford, A. A., C. M. Kuster, T. J. Schuur, A. Witt, J. Carlin, J. B. Boettcher, A. E. Reinhart, and L. J. Hopper, 2023: Examining the improved volumetric update rates afforded by dual-polarization phased array radar. 40th Conference on Radar Meteorology, Minneapolis, MN, American Meteorological Society, 9B.7.

Alford, A. A. and C. M. Kuster, 2024: Observations of tornadic mesovortices in the 27 February 2023 Central Oklahoma quasi-linear convective system. 104th Annual Meeting, Baltimore, MD, American Meteorological Society, 3.

Boettcher, J. B., F. Nai, T. J. Schuur, S. M. Torres, A. A. Alford, C. M. Kuster, and A. E. Reinhart, 2023: The NSSL ATD through NWS eyes: An assessment of base data quality. 40th Conference on Radar Meteorology, Minneapolis, MN, American Meteorological Society, 2A.6.

Bowden, K. A., and P. L. Heinselman, 2016: A Qualitative Analysis of NWS Forecasters' Use of Phased-Array Radar Data during Severe Hail and Wind Events. *Wea. Forecasting*, **31**, 43–55, doi: 10.1175/WAF-D-15-0089.1.

Burgess, D. W., L. R. Lemon, and R. A. Brown, 1975: Tornado characteristics revealed by Doppler radar. *Geophysical Research Letters*, **2**, 183-184, doi: 10.1029/GL002i005p00183.

Crum, T. D., and R. L. Alberty, 1993: The WSR-88D and the WSR-88D operational support facility. *Bull. Amer. Meteor. Soc.*, **74**, 1669–1688, doi: 10.1175/1520-0477(1993)074<1669:TWATWO>2.0.CO;2.

Dawson, D. T., E. R. Mansell, Y. Jung, L. J. Wicker, M. R. Kumjian, and M. Xue, 2014: Low-Level ZDR Signatures in Supercell Forward Flanks: The Role of Size Sorting and Melting of Hail. *J. Atmos. Sci.*, **71**, 276–299, doi: 10.1175/JAS-D-13-0118.1.

Doviak, R. J. , and D. Zrnić , 2006: Doppler Radar and Weather Observations. Dover Publications, Inc., 481 pp.

Doviak, R. J., V. Bringi, A. V. Ryzhkov, A. Zahari, and D. Zrnic, 2000: Considerations for polarimetric upgrades to operational WSR-88D radars. *Journal of Atmospheric and Oceanic Technology*, **17**, 257-278, doi: 10.1175/1520-0426(2000)017<0257:CFPUTO>2.0.CO;2.

Haberlie, A. M., and W. S. Ashley, 2019: A Radar-Based Climatology of Mesoscale Convective Systems in the United States. *J. Climate*, **32**, 1591–1606, doi: 10.1175/JCLI-D-18-0559.1.

Heinselman, P. L., Priegnitz D. L. , Manross K. L. , Smith T. M. , and Adams R. W. , 2008: Rapid sampling of severe storms by the National Weather Radar Testbed Phased Array Radar. *Wea. Forecasting*, **23**, 808–824, doi:10.1175/2008WAF2007071.1.

Heinselman, P. L., D. S. LaDue, and H. Lazrus, 2012: Exploring impacts of rapid-scan radar data on NWS warning decisions. *Wea. Forecasting*, **27**, 1031–1044, doi: 10.1175/WAF-D-11-00145.1.

Heinselman, P. L., D. S. LaDue, D. M. Kingfield, and R. Hoffman, 2015: Tornado warning decisions using phased-array radar data. *Wea. Forecasting*, **30**, 57–78, doi: 10.1175/WAF-D-14-00042.1.

Ivić, I., R. Mendoza, D. Schvartzman, S. Torres, and D. Wasielewski, 2020: Preliminary report on polarimetric calibration for the Advanced Technology Demonstrator, NOAA/NSSL report, 34 pp. https://nssl.noaa.gov/publications/par_reports/.

Ivić, I., F. Nai, and S. Torres, 2023: An update on polarimetric calibration for the Advanced Technology Demonstrator, NOAA/NSSL report, 74 pp. (to be posted to https://nssl.noaa.gov/publications/par_reports/ later in 2024).

Kingfield, D. M., and M. M. French, 2022: The Influence of WSR-88D Intra-Volume Scanning Strategies on Thunderstorm Observations and Warnings in the Dual-Polarization Radar Era: 2011–20. *Wea. Forecasting*, **37**, 283–301, doi: 10.1175/WAF-D-21-0127.1.

Kuster, C. M., P. L. Heinselman, and T. J. Schuur, 2016: Rapid-Update Radar Observations of Downbursts Occurring within an Intense Multicell Thunderstorm on 14 June 2011. *Wea. Forecasting*, **31**, 827–851, doi: 10.1175/WAF-D-15-0081.1.

Kuster, C. M., J. C. Snyder, T. J. Schuur, T. T. Lindley, P. L. Heinselman, J. C. Furtado, J. W. Brogden, and R. Toomey, 2019: Rapid-Update Radar Observations of ZDR Column Depth and Its Use in the Warning Decision Process. *Wea. Forecasting*, **34**, 1173–1188, doi: 10.1175/WAF-D-19-0024.1.

Kuster, C. M., B. R. Bowers, J. T. Carlin, T. J. Schuur, J. W. Brogden, R. Toomey, and A. Dean, 2021: Using KDP Cores as a Downburst Precursor Signature. *Wea. Forecasting*, **36**, 1183–1198, doi: 10.1175/WAF-D-21-0005.1.

Kuster, C. M., K. Sherburn, V. Mahale, T. J. Schuur, O. McCauley, and J. Schaumann, 2023: Dual-polarization radar signatures associated with QLCS mesovortices. 40th Conference on Radar Meteorology, Minneapolis, MN, American Meteorological Society, 16A.7.

McAnelly, R. L., J. E. Nachamkin, W. R. Cotton, and M. E. Nicholls, 1997: Upscale Evolution of MCSs: Doppler Radar Analysis and Analytical Investigation. *Mon. Wea. Rev.*, **125**, 1083–1110, doi: 10.1175/1520-0493(1997)125<1083:UEOMDR>2.0.CO;2.

Newman, J. F., and P. L. Heinselman, 2012: Evolution of a Quasi-Linear Convective System Sampled by Phased Array Radar. *Mon. Wea. Rev.*, **140**, 3467–3486, doi: 10.1175/MWR-D-12-00003.1.

Pazmany, A. L., J. B. Mead, H. B. Bluestein, J. C. Snyder, and J. B. Houser, 2013: A Mobile Rapid-Scanning X-band Polarimetric (RaXPol) Doppler Radar System. *J. Atmos. Oceanic Technol.*, **30**, 1398–1413, doi: 10.1175/JTECH-D-12-00166.1.

Palmer, R., and Coauthors, 2022: A Primer on Phased Array Radar Technology for the Atmospheric Sciences. *Bull. Amer. Meteor. Soc.*, **103**, E2391–E2416, doi: 10.1175/BAMS-D-21-0172.1.

Reinhart, A. E., S. M. Torres, D. Wasielewski, T. J. Schuur, R. Mendoza, L. J. Hopper, and K. D. Hondl, 2023: An update of the phased array research program at the National Severe Storms Laboratory. 40th Conference on Radar Meteorology, Minneapolis, MN, American Meteorological Society, 9B.1.

Ryzhkov, A., T. J. Schuur, D. W. Burgess, and D. S. Zrnic, 2005: Polarimetric tornado detection. *Journal of Applied Meteorology*, **44**, 557-570, doi: 10.1175/JAM2235.1.

Schuur, T. J., C. M. Kuster, A. A. Alford, J. B. Boettcher, A. Witt, J. Carlin, A. E. Reinhart, and L. J. Hopper, 2023: Spring 2023 data collection with the NSSL Advanced Technology Demonstrator (ATD) phased array radar. 40th Conference on Radar Meteorology, Minneapolis, MN, American Meteorological Society, 9B.2.

Segall, J. H., M. M. French, D. M. Kingfield, S. D. Loeffler, and M. R. Kumjian, 2022: Storm-Scale Polarimetric Radar Signatures Associated with Tornado Dissipation in Supercells. *Wea. Forecasting*, **37**, 3–21, doi: 10.1175/WAF-D-21-0067.1.

Stailey, J. E., and K. D. Hondl, 2016: Multifunction phased array radar for aircraft and weather surveillance. *Proc. IEEE*, **104**, 649–659, doi: 10.1109/JPROC.2015.2491179.

Steward, E. B., C. M. Kuster, A. A. Alford, T. J. Schuur, and V. N. Mahale, 2023: Comparing differential reflectivity arcs using phased array and convection radar data. National Weather Center Research Experience for Undergraduates Report, 10 pp, https://caps.ou.edu/reu/reu23/finalpapers/Steward_FinalPaper.pdf.

Stratman, D. R., N. Yussouf, Y. Jung, T. A. Supinie, M. Xue, P. S. Skinner, and B. J. Putnam, 2020: Optimal temporal frequency of NSSL phased-array radar observations for an experimental warn-on-forecast system. *Wea. Forecasting*, **35**, 193–214, doi: 10.1175/WAF-D-19-0165.1.

Supinie, T. A., N. Yussouf, Y. Jung, M. Xue, J. Cheng, and S. Wang, 2017: Comparison of the analyses and forecasts of a tornadic supercell storm from assimilating phased-array radar and WSR-88D observations. *Wea. Forecasting*, **32**, 1379–1401, doi: 10.1175/WAF-D-16-0159.1.

Torres, S. M., and Coauthors, 2016: Adaptive-weather-surveillance and multifunction capabilities of the National Weather Radar Testbed phased array radar. *Proc. IEEE*, **104**, 660–672, doi: 10.1109/JPROC.2015.2484288.

Torres, S. M. and D. Wasielewski, 2022: The Advanced Technology Demonstrator at the National Severe Storms Laboratory: Challenges and Successes. IEEE Radar Conference, New York City, NY, IEEE, 1-6, doi: 10.1109/RadarConf2248738.2022.9764231.

Wilson, K. A., P. L. Heinselman, C. M. Kuster, D. M. Kingfield, and Z. Kang, 2017: Forecaster performance and workload: Does radar update time matter? *Wea. Forecasting*, **32**, 253–274, doi: 10.1175/WAF-D-16-0157.1

Zrnić, D., and Coauthors, 2007: Agile-beam phased array radar for weather observations. *Bull. Amer. Meteor. Soc.*, **88**, 1753–1766, doi: 10.1175/BAMS-88-11-1753.